AD-A031 609   AIR FORCE AERO PROPULSION LAB WRIGHT-PATTERSON AFB OHIO   F/G 20/11
TRANSIENT RESPONSE OF A CANTILEVERED PLATE TO IMPACT USING HOLO--ETC(U)
AUG 76   J C MACBAIN
UNCLASSIFIED   AFAPL-TR-76-56   NL

| OF |

AD
A031609

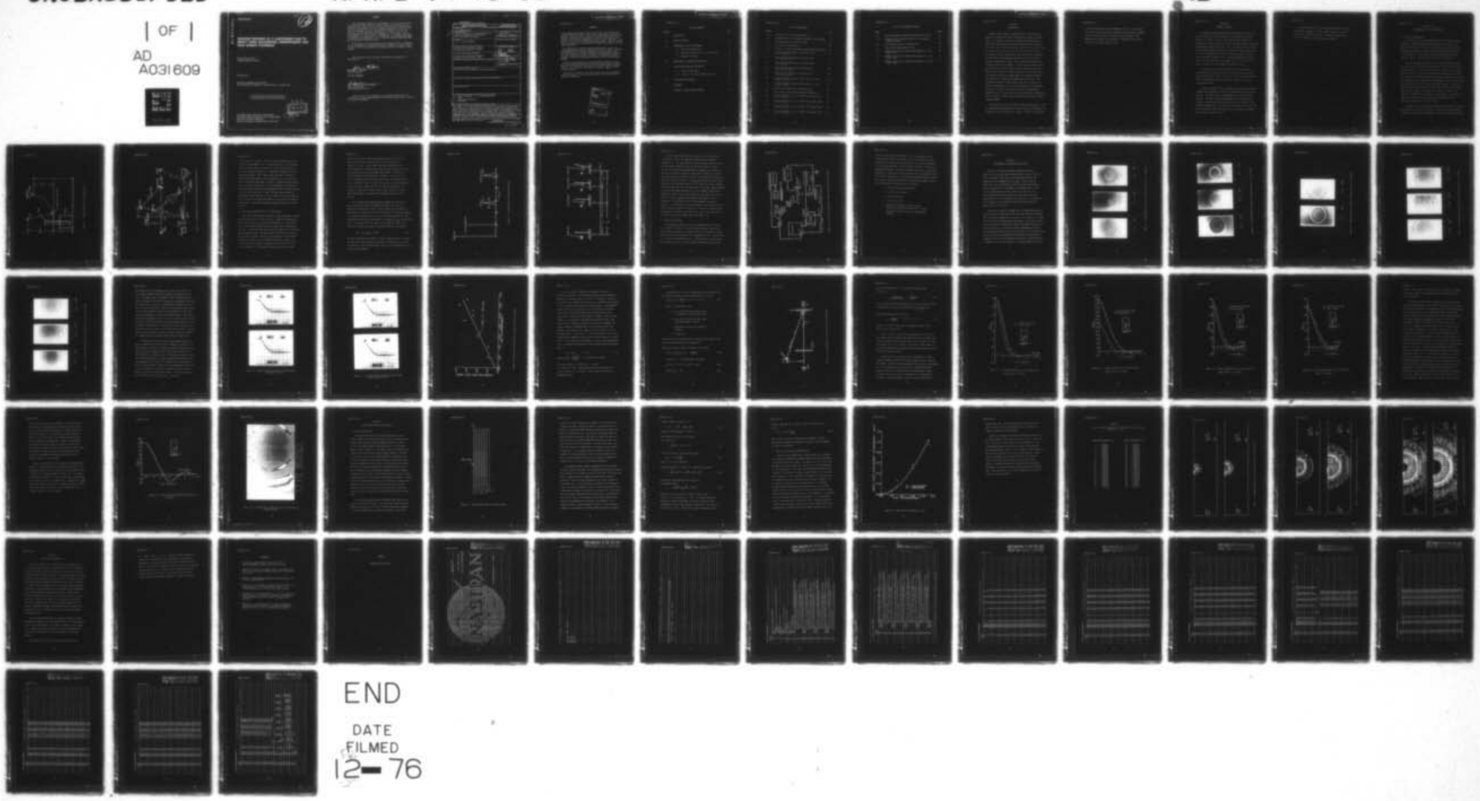

END
DATE
FILMED
12-76

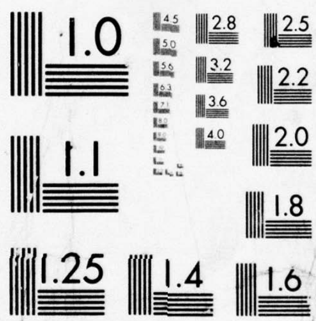

MICROCOPY RESOLUTION TEST CHART

NATIONAL BUREAU OF STANDARDS-1963-A

AFAPL-TR-76-56

TRANSIENT RESPONSE OF A CANTILEVERED PLATE TO IMPACT USING HOLOGRAPHIC INTERFEROMETRY AND FINITE ELEMENT TECHNIQUES

PROPULSION BRANCH
TURBINE ENGINE DIVISION

AUGUST 1976

TECHNICAL REPORT AFAPL-TR-76-56
FINAL REPORT FOR PERIOD 1 JANUARY 1976 TO 1 AUGUST 1976

AIR FORCE AERO PROPULSION LABORATORY
AIR FORCE WRIGHT AERONAUTICAL LABORATORIES
AIR FORCE SYSTEMS COMMAND
WRIGHT-PATTERSON AIR FORCE BASE, OHIO 45433

NOTICE

When Government drawings, specifications, or other data are used for any purpose other than in connection with a definitely related Government procurement operation, the United States Government thereby incurs no responsibility nor any obligation whatsoever; and the fact that the Government may have formulated, furnished, or in any way supplied the said drawings, specifications, or other data, is not to be regarded by implication or otherwise as in any manner licensing the holder or any other person or corporation, or conveying any rights or permission to manufacture, use, or sell any patented invention that may in any way be related thereto.

This report has been reviewed by the Information Office (ASD/OIP), and is releasable to the National Technical Information Service (NTIS). At NTIS, it will be available to the general public, including foreign nations.

This technical report has been reviewed and is approved for publication.

James C. MacBain

DR. JAMES C. MACBAIN
Project Engineer

FOR THE COMMANDER

I.J. Gershon

I.J. GERSHON, Tech Area Manager
Propulsion Branch
Turbine Engine Division

Copies of this report should not be returned unless return is required by security considerations, contractual obligations, or notice on a specific document.

AIR FORCE - 15 OCTOBER 76 - 100

(9) Final rept. 1 Jan-1 Aug 76

UNCLASSIFIED

SECURITY CLASSIFICATION OF THIS PAGE (When Data Entered)

REPORT DOCUMENTATION PAGE

READ INSTRUCTIONS BEFORE COMPLETING FORM

1. REPORT NUMBER (14) AFAPL-TR-76-56

2. GOVT ACCESSION NO.

3. RECIPIENT'S CATALOG NUMBER

4. TITLE (and Subtitle) (6)
Transient Response of a Cantilevered Plate to Impact Using Holographic Interferometry and Finite Element Techniques.

5. TYPE OF REPORT & PERIOD COVERED
Final Report
1 January 76 - 1 August 76

6. PERFORMING ORG. REPORT NUMBER

7. AUTHOR(s) (10)
James C. MacBain

8. CONTRACT OR GRANT NUMBER(s)

9. PERFORMING ORGANIZATION NAME AND ADDRESS
Air Force Aero Propulsion Laboratory
Wright-Patterson AFB, Ohio 45433

10. PROGRAM ELEMENT, PROJECT, TASK AREA & WORK UNIT NUMBERS
646100 306612
3066 30661221

11. CONTROLLING OFFICE NAME AND ADDRESS
Air Force Aero Propulsion Laboratory
Wright-Patterson AFB, Ohio 45433

12. REPORT DATE (11)
Aug[redacted]76

13. NUMBER OF PAGES
64 (12) 71p.

14. MONITORING AGENCY NAME & ADDRESS (if different from Controlling Office)

15. SECURITY CLASS. (of this report)
Unclassified

15a. DECLASSIFICATION/DOWNGRADING SCHEDULE

16. DISTRIBUTION STATEMENT (of this Report)
Approved for Public Release, Distribution Unlimited

17. DISTRIBUTION STATEMENT (of the abstract entered in Block 20, if different from Report)

18. SUPPLEMENTARY NOTES

19. KEY WORDS (Continue on reverse side if necessary and identify by block number)
1. Transient Response
2. Impact
3. Finite Element Analysis
4. Holography
5. Cantilevered Plate

20. ABSTRACT (Continue on reverse side if necessary and identify by block number)
This report covers work carried out at AFAPL's Turbo Structures Research Laboratory (TSRL) on the transient structural response of an isotropic cantilevered plate subjected to normal impact by a ballistic pendulum. The program was a combined experimental/analytical effort. The experimental portion utilized a pulsed ruby laser to obtain holographic interferograms of the plate's deformation following impact. The analytical portion of the work consisted of mathematically modelling the plate using finite element techniques and studying the model's response to impact using the general purpose finite element program, NASTRAN.

DD FORM 1 JAN 73 1473 EDITION OF 1 NOV 65 IS OBSOLETE

UNCLASSIFIED

SECURITY CLASSIFICATION OF THIS PAGE (When Data Entered)

011 570

FOREWORD

This report covers work carried out at AFAPL's Turbo Structures Research Laboratory (TSRL) on the transient structural response of an isotropic cantilevered plate subjected to normal impact by a ballistic pendulum. The effort was intended as a vehicle for evaluating the methods of pulsed laser holography and finite element analysis as they relate to the study of transient structural dynamics. This is an area which bears directly on the problem of foreign object damage to turbine engine components.

The program was a combined expermental/analytical effort. The experimental portion utilized a pulsed ruby laser to obtain holographic interferograms of the plate's deformation following impact. The analytical portion of the work consisted of mathematically modelling the plate using finite element techniques and studying the model's response to impact using the general purpose finite element program, NASTRAN.

The work was performed in the Turbine Engine Division of the Air Force Aero Propulsion Laboratory, Air Force Systems Command, Wright-Patterson Air Force Base, Ohio under Project 3066, Task 12, and Work Unit 21. The effort was conducted by Dr. James C. MacBain of the Propulsion Branch.

The author is indebted to Mr. Bruce Tavner for his very competent technical assistance in the laboratory and to Miss Helen Davis for typing the manuscript.

TABLE OF CONTENTS

LIST OF ILLUSTRATIONS

LIST OF ILLUSTRATIONS (CONT'D)

SECTION I

INTRODUCTION

Foreign object damage in both military and civilian turbine engines is a seldom but serious problem both in terms of cost and safety. For example, the Air Force Inspection and Safety Center states that 2816 birdstrikes have been reported Air Force-wide between 1966 and 1973. These birdstrikes resulted in a loss of 7 lives, 14 aircraft, and a cost to the Air Force of $74 million dollars. These figures serve to underline the fact that there is a definite need for both basic and applied research in the area of impact-tolerant turbine engine blading. More sophisticated design tools and impact theories are required. In this vein, this report covers work carried out at AFAPL's Turbo Structures Research Laboratory (TSRL) on the transient structural response of an isotropic cantilevered plate subjected to normal impact by a ballistic pendulum. The program was a combined experimental/analytical effort. The experimental portion utilized a pulsed ruby laser to obtain holographic interferograms of the plate's deformation following impact. The analytical portion of the work consisted of mathematically modelling the plate using finite element techniques and studying the model's response to impact using the general purpose finite element program, NASTRAN.

The specific aims of this research effort were threefold. First, the advantages and disadvantages of using pulsed laser holography for transient structural analysis were studied. Second, it was intended to use the experimental pulsed holography results as a verification of results obtained analytically using the computer program, NASTRAN. Finally, the research effort served to provide knowledge of and experience with pulsed laser holography - information that will be useful in future TSRL research efforts.

SECTION II

SUMMARY OF RESULTS

An aluminum cantilevered plate measuring 3"x7"x.1875" was struck with a ballistic pendulum consisting of a .65" diameter steel ball attached to a wire on a pivot. The resulting plate response was measured for a specified time after impact by double exposure holographic interferometry using a pulsed ruby laser. The plate's normal displacement was experimentally determined for times after impact ranging from 2 to 33μs. Photographs of the double exposure holograms from these tests are shown in Figures 4.1-4.5. The normal displacement based on four of the test runs (times after impact of 4, 6, 12, and 18μs) is shown as a function of plate geometry in Figures 4.10-4.13.

The flexural wave velocity was computed from the holographic interferograms by plotting the plate wave position versus time after impact and was found to be C_f = .102 in/μs. This is in good agreement with the theoretical Rayleigh surface wave velocity of .112 in/μs - a difference of 8.5%.

A parallel numerical study was conducted using the finite element computer program NASTRAN to compute the cantilevered plate's transient response. The results were in good agreement with the experimental findings. The plate's normal displacement based on finite element analysis is shown plotted in Figures 4.10-4.13 as a function of plate geometry (dashed lines). Contour plots of the plate's normal displacement for different times after impact were also generated by NASTRAN and are shown in Figures 5.3-5.5.

The study demonstrated the feasibility and utility of using pulsed laser holography to study transient structural response. In addition, it provided increased confidence and experience in the use of NASTRAN's transient analysis capability.

SECTION III

EXPERIMENTAL SET UP AND PROCEDURE

3.1 Physical Configuration

The test piece for the experimental portion of the impact analysis program was a 6061-T6 aluminum plate measuring 12" in length, 3" in width, and 3/16" thick. The plate was fixed between two steel blocks having a total weight of 33 lbf such that it was cantilevered and had a free length of 7". The weight of the cantilevered portion of the plate was .394 lbf. The plate and jig are shown in Figure 3.1.

The plate was impacted normally by a steel ball weighing .043 lbf at a point lying on its long axis and located 3" above its fixed end as shown in Figure 3.1. The ball was soldered to a thin wire that in turn was fixed to a pivot located a distance above the impact point forming what is known as a ballistic pendulum. The impact sequence was initiated by suspending the steel ball from an electromagnet which was then switched off allowing the ball to swing down and strike the plate. Just prior to impact, the ball interrupted a continuous wave laser beam passing behind the plate (see Figure 3.2) causing a photo diode to transmit a 10V signal that initiated the pulsed laser firing sequence. The timing and electronics involved in the pulsed laser firing sequence will be addressed in more detail in a later section.

The optical set up for making the hologram is also shown in Figure 3.2. The placement of the optics is typical of that used to make transmission holograms with an off-axis holographic set up, and the reader is referred

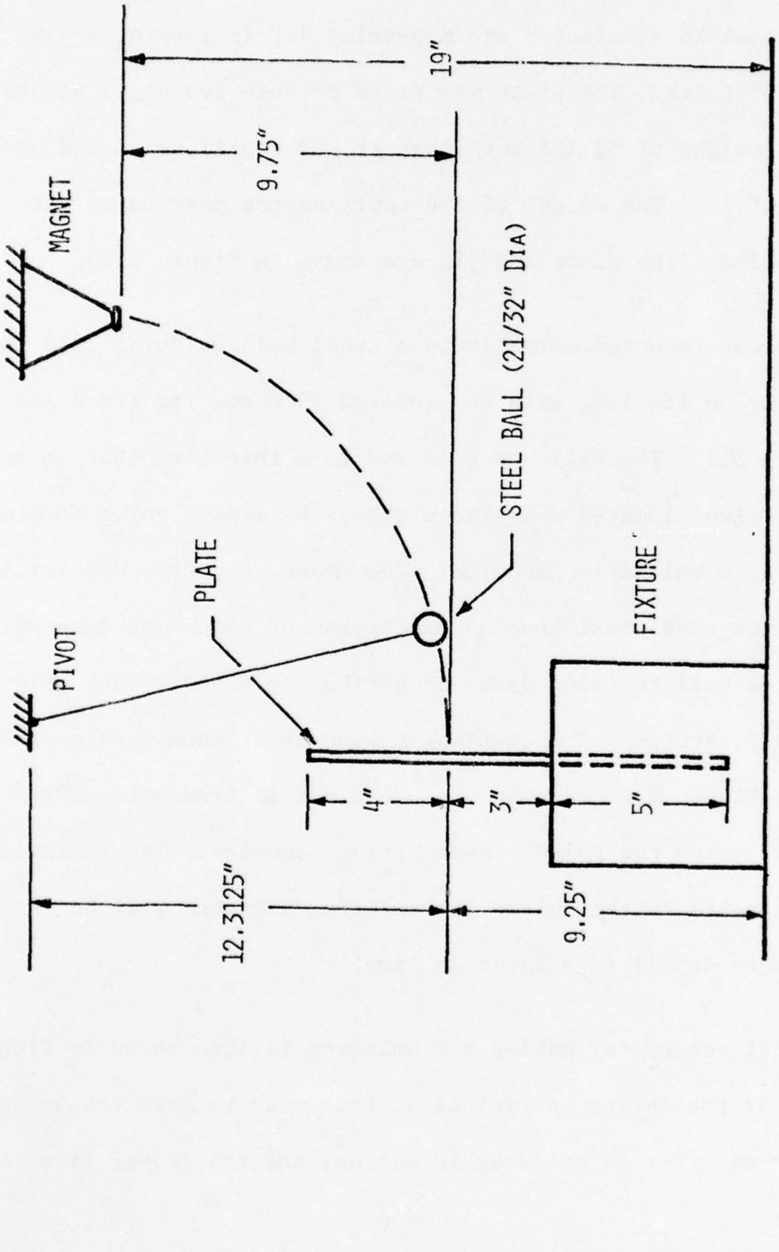

Figure 3.1 - Cantilever Plate and Pendulum Geometry

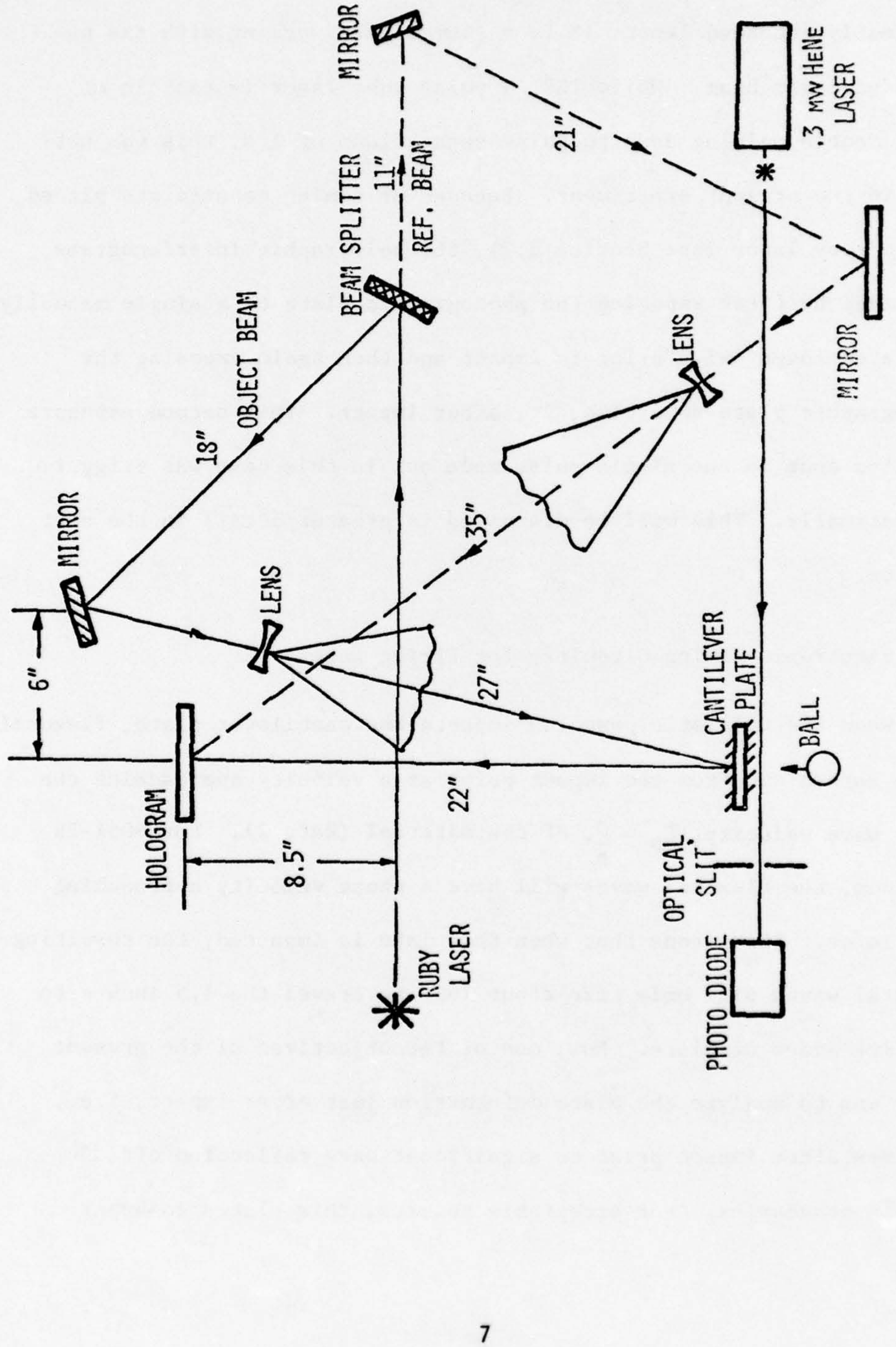

Figure 3.2 - Experimental Set-up for Making Holographic Interferograms

to Reference 1 for details. The holograms were made using a pulsed ruby laser (Apollo Model 22HD). The laser puts out 2.5 joules/pulse, 20-50ns in width, which necessitates the use of dielectric mirrors and doubly concaved lenses (F.L. = -40mm) when working with the unexpanded laser beam. While TSRL's pulse ruby laser is capable of rapid double pulsing down to pulse separations of 1μs, this was not done in the present experiment. Because of timing constraints placed on the ruby laser (see Section 3.2), the holographic interferograms were made by first exposing the photographic plate to a single manually initiated laser pulse prior to impact and then again exposing the photographic plate some time, Δt, after impact. This second exposure was also done in the single pulse mode but in this case was triggered automatically. This will be discussed in greater detail in the next section.

3.2 Electronic Timing Circuitry for Firing Laser

When the ballistic pendulum impacts the cantilever plate, flexural waves spread out from the impact point at a velocity approaching the shear wave velocity, $C_s = \frac{G}{\rho}$, of the material (Ref. 2). For 6061-T6 aluminum, the flexural waves will have a phase velocity approaching .114 in/μs. This means that when the plate is impacted, the resulting flexural waves will only take about 16μs to travel the 1.5 inches to the free sides of plate. Now, one of the objectives of the present study was to analyze the plate deformation just after impact, i.e., at times after impact <u>prior</u> to significant wave reflection off the plate's boundaries. For acceptable results, this places an upper bound on the time for firing the second laser pulse of about 30μs (wave reflection will occur off the closest free edges of the plate at t ≐ 16μs). This in turn places some constraints on the firing sequence for the ruby laser since, as shown in Figure 3.3, the ruby laser can fire only after 200μs have elapsed - the amount of time necessary for the flash lamps to energize. This is true for either the single pulse, as in the present case, or the double pulse mode of operation. Hence, in order for the laser to lase automatically at some time after impact in the 0-30μs range, it would have to be triggered (signal sent to Master Sync) at some time prior to impact. This was done using a timing delay oscilloscope (Tektronix 535) as follows.

Prior to making the double exposure hologram, the time that it took the ball to go from the trigger laser beam to the plate was measured by an electronic counter. This is shown as T_{AC} in Figure 3.4. This distance traversed by the ball in going from A to C was approximately 1 inch and T_{AC} was typically in the .02 second range (20,000μs). Upon specifying the time after plate impact to be observed, T_{IMPT}, and utilizing the fact that Pulse #2 of the laser fires at 1000μs into the firing sequence, the delay time, T_{AB}, was determined from the relationship:

$$T_{AB} = T_{AC} + T_{IMPT} - 1000\mu s \tag{3.1}$$

The delay oscilloscope was then set so that a signal was sent to trigger the ruby laser after a delay of T_{AB} seconds. The Pockels cell voltage for Pulse #1 of the ruby laser was set to zero, thus eliminating Pulse #1 from the firing sequence.

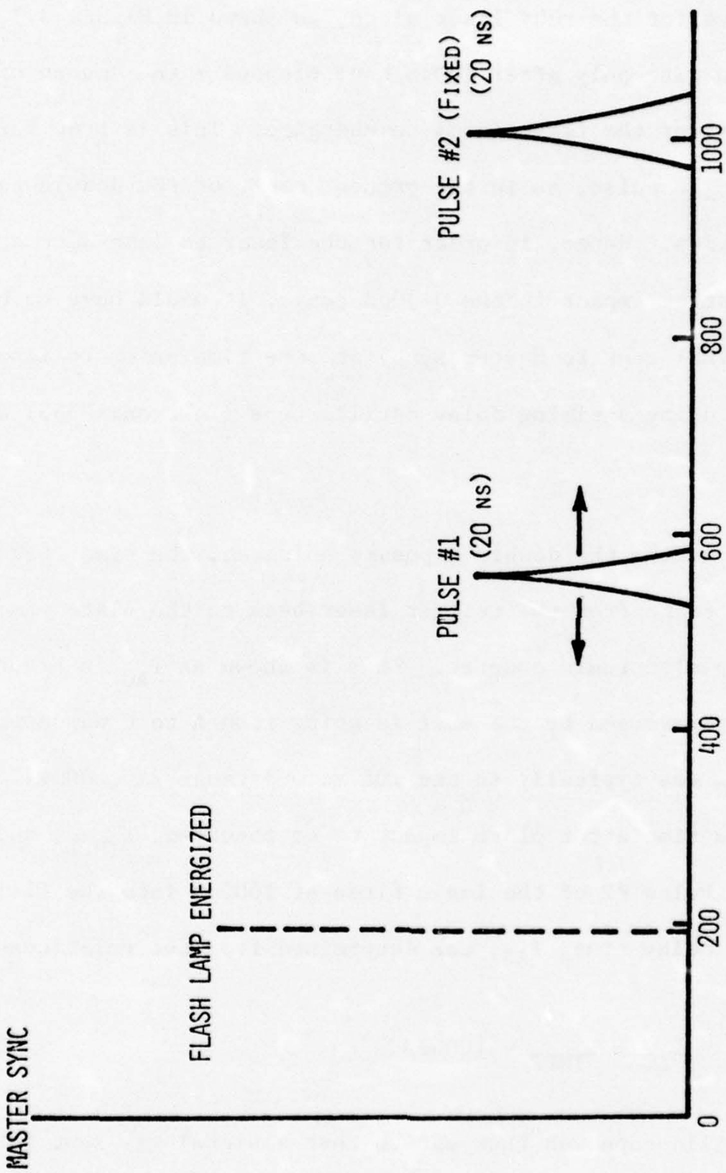

Figure 3.3 - Timing Sequence for Pulsed Ruby Laser

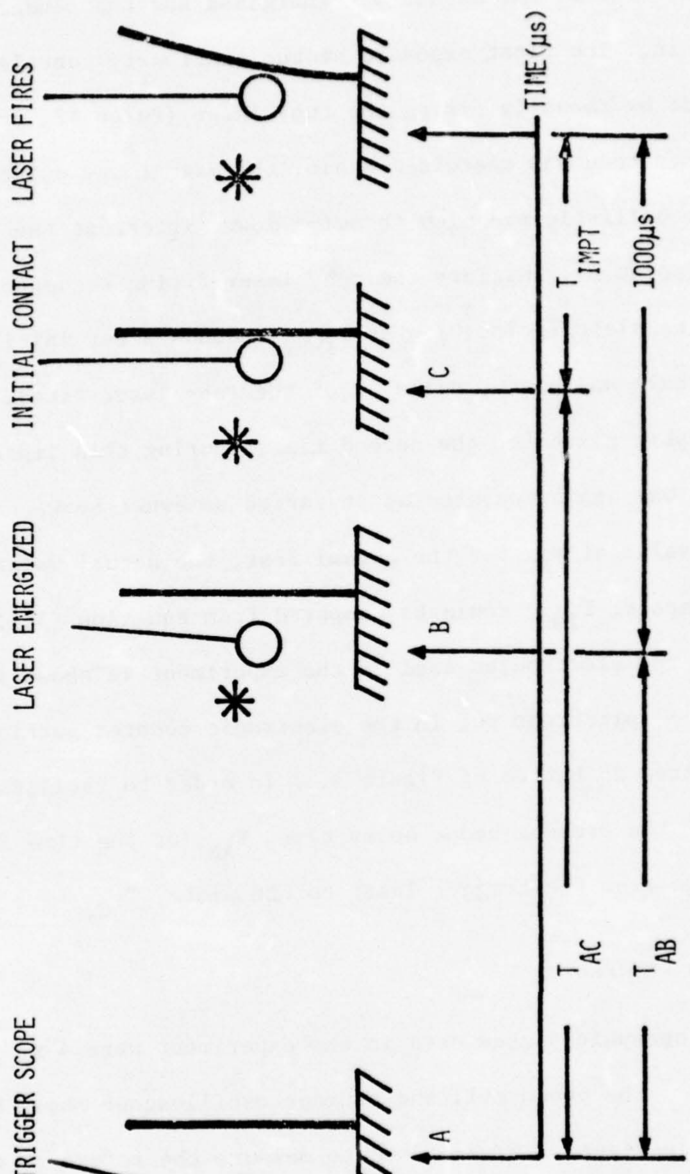

Figure 3.4 - Impact/Laser Timing Sequence

With the steps mentioned above carried out, the actual impact test was run. First, the magnet was energized and the pendulum attached to it. The first exposure of the stationary cantilever plate was then made by manually firing the ruby laser (Pulse #2, only). The ruby laser then was energized again, the magnet was switched off, allowing the ballistic pendulum to swing down, interrupt the trigger laser beam (point A), initiate the ruby laser firing sequence (point B), and impact the plate (point C). At T_{IMPT} seconds after initial contact between the ball and plate, Pulse #2 of the ruby laser fired, exposing the photographic plate for the second time. During this impact sequence, the time T_{AC} was again measured as it varied somewhat between tests. Knowing the value of T_{AC} for the actual test, the actual value of the time after impact, T_{IMPT} could be computed from equation (3.1). A schematic of the electronics used in the experiment is shown in Figure 3.5. A switch was put in the electronic counter portion of the circuit (located at bottom of Figure 3.5) in order to facilitate quick monitoring of the present scope delay time, T_{AB}, or the time it took the ball to go from the trigger laser to the plate, T_{AC}.

3.3 Hologram Processing

The photographic plates used in the experiment were 4"x5" Agfa-Gevaert 10E75. The photo cell and storage oscilloscope shown behind the hologram in Figure 3.5 were used to measure the reference to object beam ratio and pulse amplitude of the holographic set up. The beam ratio for the tests was approximately 2 to 1 (reference beam to object beam). The combination of photo cell and storage oscilloscope could only give

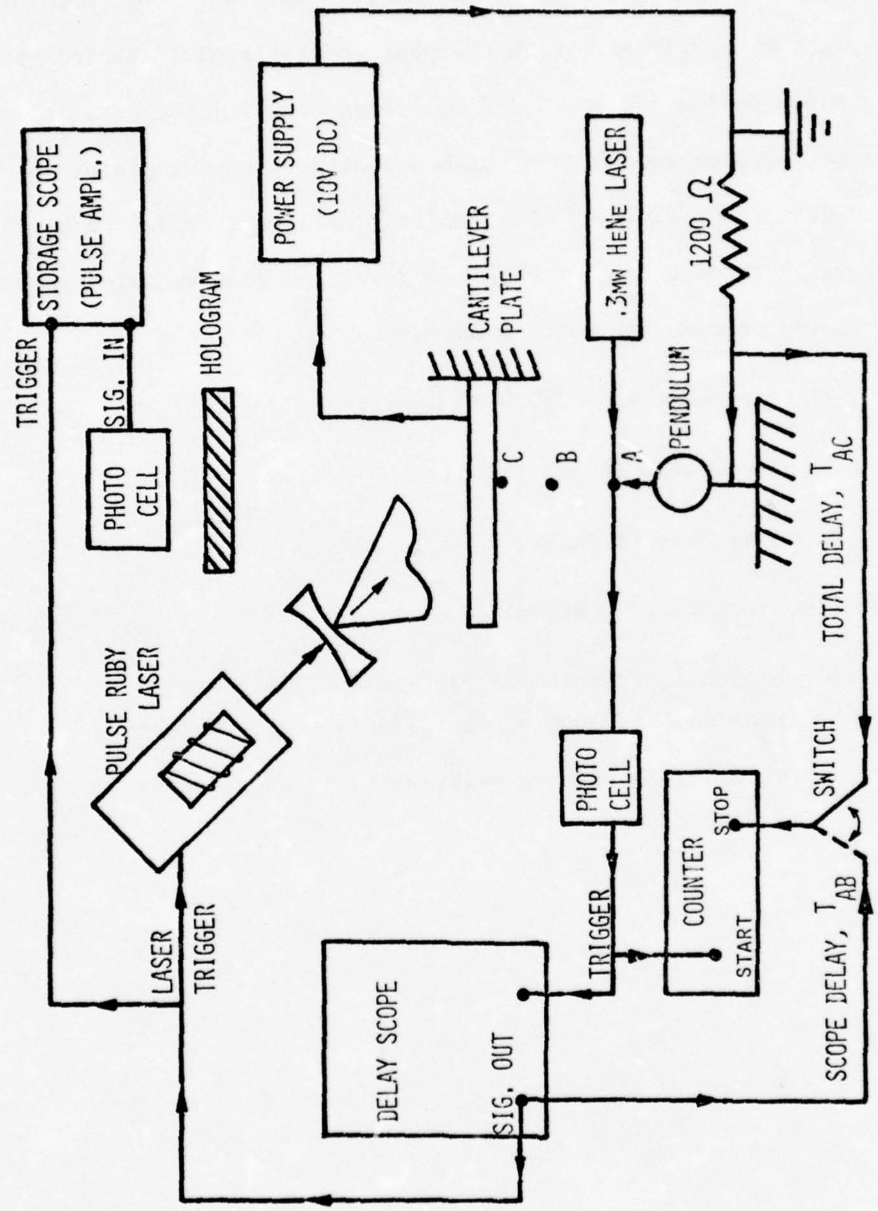

Figure 3.5 - Electronic Circuitry for Making a Double Exposure Hologram

relative light intensity measurements, i.e., the amplitude of the reference beam relative to the object beam or the relative amplitude between the first and second plate exposures. This sufficed, however, for the present experiment. With the photo cell placed 1" behind the hologram plate holder, "acceptable" holograms resulted for oscilloscope readings of .4 volts and .6 volts with and without a photographic plate in the holder, respectively. The resulting holograms tended to be dark but this was corrected by bleaching the developed photographic plates. The developing process was carried out as follows:

1. 4 minutes in Kodak D-19 developer;
2. 30 seconds in stop bath;
3. 3 minutes in fixer;
4. Dry with blow dryer;
5. Bleach in Potasium Ferricynanide (15g of $K_3Fe(CN)_6$ in 1000 ml distilled water) - agitate until plate becomes milky white, approximately 1 minute.

SECTION IV

EXPERIMENTAL DATA REDUCTION AND RESULTS

Figures 4.1 through 4.5 show the cantilevered plate's response for times after impact ranging from 2μs to 33μs. For the sake of increased fringe clarity, the photographs taken of the holograms show the immediate area of impact. Recall that the impact point lies on the vertical axis of the plate and 3 inches above the clamped base. The numbers in parentheses refer to the raw data numbering system used to denote each test run. The 6061-T6 aluminum plate was painted with a flat white paint and a grid having 1" by .5" increments was scribed on it. In addition, 1/8" increments were scribed on the plate centerline from the impact point to 1" below it.

Referring to Figures 4.1 through 4.5, the fringes concentrically located around the impact point (ball impacting from rear) represent loci of constant displacement on the plate. The fringes are a contour map of the flexural waves caused by the impact. They travel outward with time until they reach the free edge of the plate at about T=12μs and are reflected. It is evident from the photographs that either the timing measurements are in error by as much as ± 2μs or that there was some scatter in the magnitude and duration of the impulse load imparted to the plate by the steel ball pendulum. The latter reason is thought to be the case because of a permanent magnetic field that

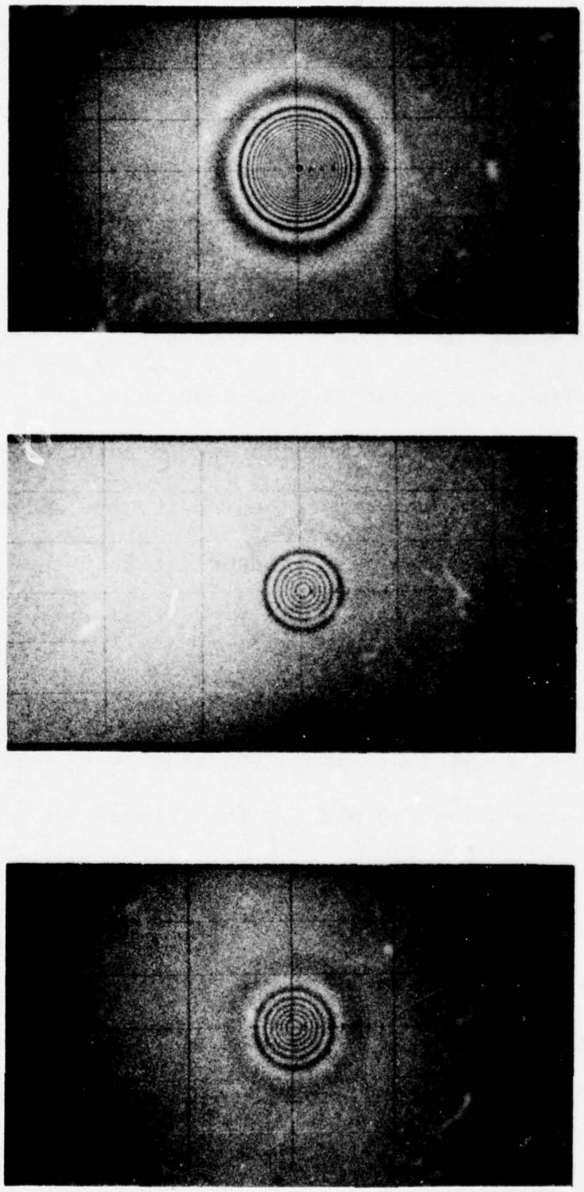

2 μs (91) 4 μs (89) 6 μs (90)

Figure 4.1 - Double Exposure Holograms of Cantilever Plate (2, 4, and 6μs)

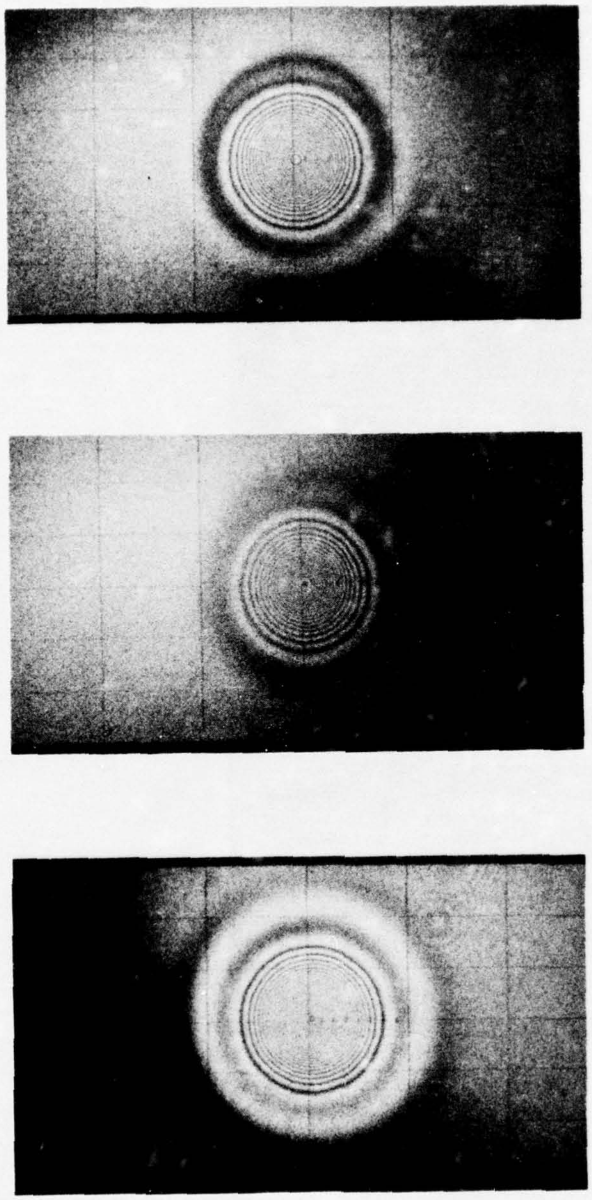

9 µs (101)

10 µs (98)

11 µs (95)

Figure 4.2 - Double Exposure Holograms of Cantilever Plate (9, 10, and 11µs)

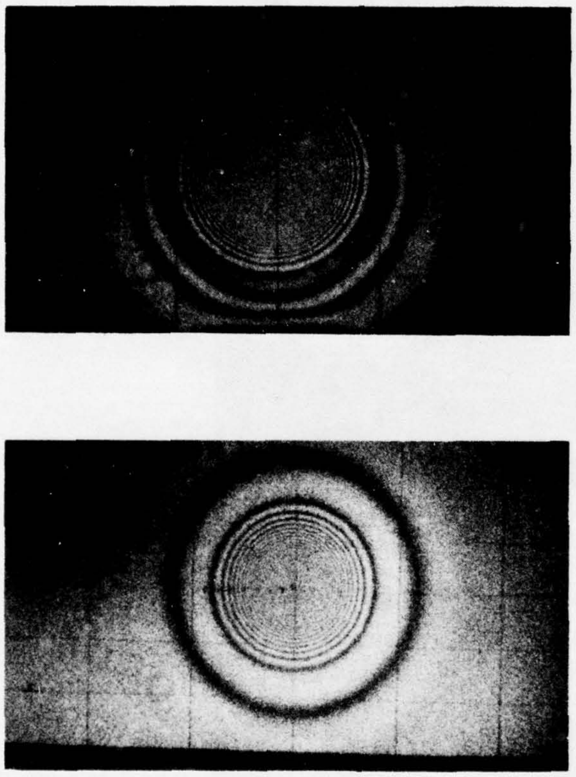

12 μs (107)   13 μs (96)

Figure 4.3 - Double Exposure Holograms of Cantilever Plate (12 and 13μs)

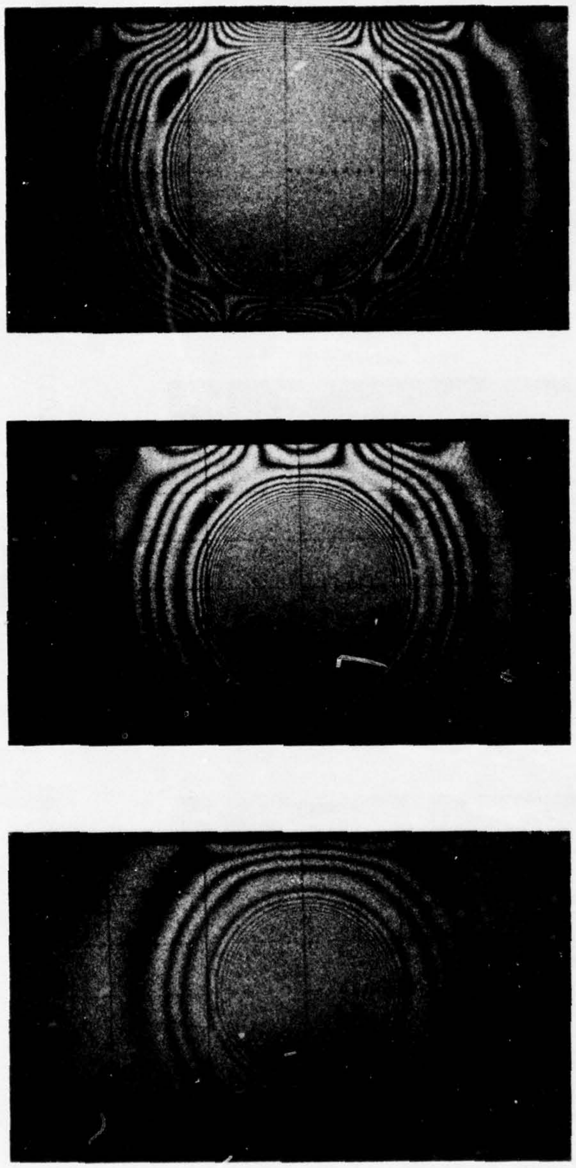

16 μs (93)

18 μs (106)

24 μs (108)

Figure 4.4 - Double Exposure Hologram of Cantilever Plate (16, 18, and 24μs)

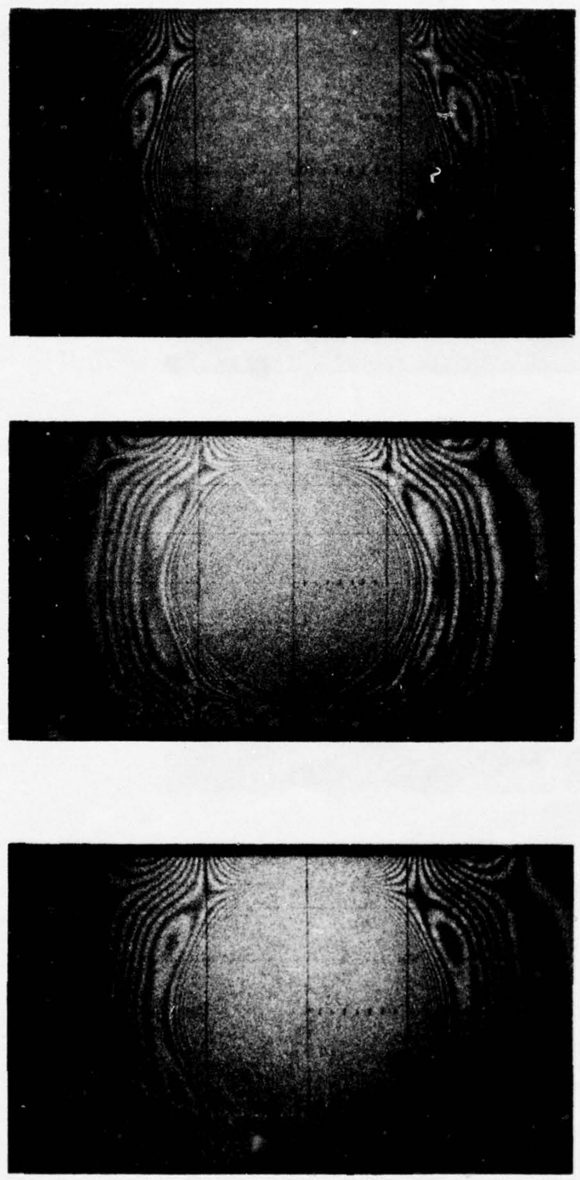

28 µs (110) 30 µs (105) 33 µs (103)

Figure 4.5 - Double Exposure Hologram of Cantilever Plate (28, 30, and 33µs)

was induced in the electromagnet used to release the steel ball. The permanent magnetic field varied somewhat throughout the duration of the impact tests. The magnetic force field would have the effect of slowing up the ball's release and, consequently, decreasing its impact force. This fact is corroborated by Figures 4.6 and 4.7 where the force time profile is seen for four successive ball impacts on a pressure transducer (Piezotronics, PCB 118A-B, 2μs rise time) temporarily imbedded in the plate at the impact point. The pressure amplitude (proportional to force) in test 1 is 20% less than the tests 2 through 4. While future work in this area should strive for a more repeatable loading system, the present data scatter was found to be acceptable within the scope of the present research effort. The load profile shown in Figures 4.6 and 4.7 was also utilized to determine the loading input for the finite element analysis (Section 5.1).

The fringe pattern position and the corresponding times after impact in Figures 4.1-4.5 can be used to compute the velocity of the flexural waves in the plate. Using the outermost visible fringe for times after impact ranging from 2μs to 13μs, one can get a plot of wave position as a function of time. The slope of this curve will be the flexural wave velocity. Using the fringe pattern positions and corresponding times in Figures 4.1 through 4.3, the curve shown in Figure 4.8 was generated. Because of the aforementioned scatter due to load repeatability, a linear least squares routine was used to generate the curve through the data points. The slope of the curve gives the flexural wave velocity as $C_f = .1024$ in/μs.

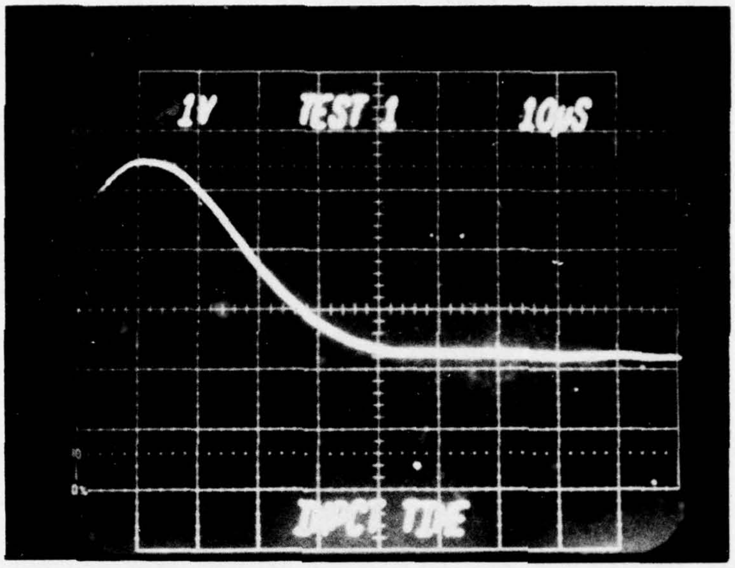

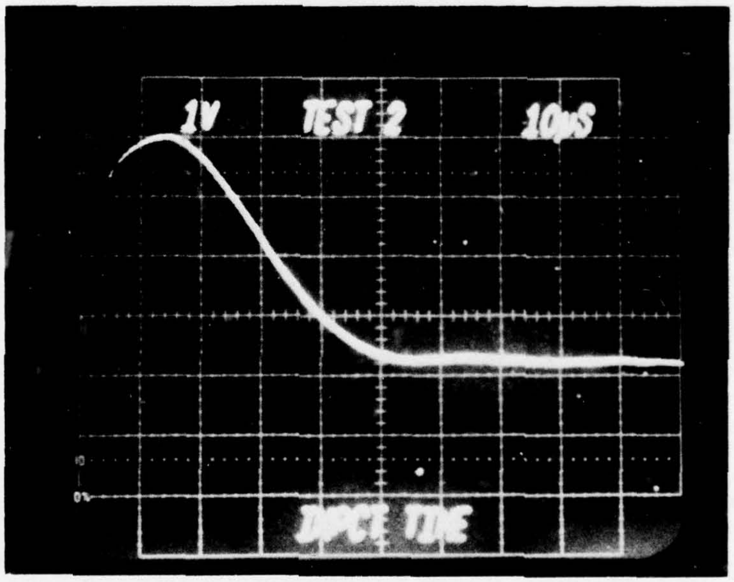

Figure 4.6 - Pressure Transducer Output at Impact Point Vs Time (Tests 1 and 2)

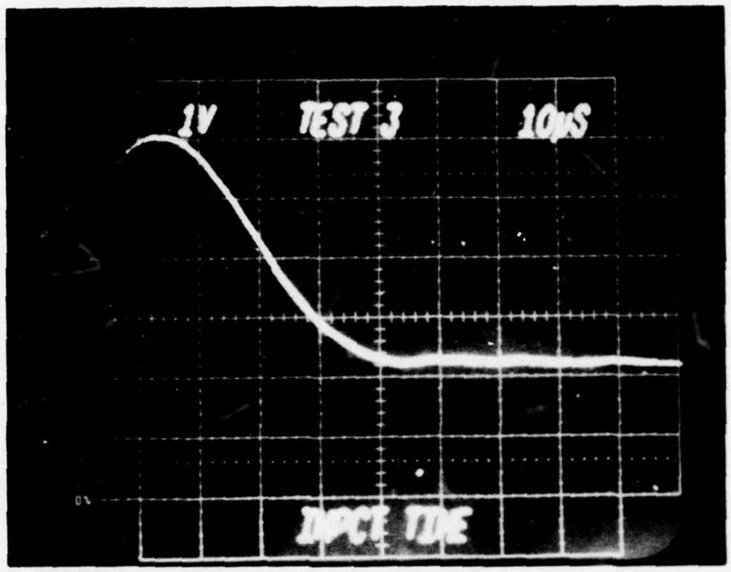

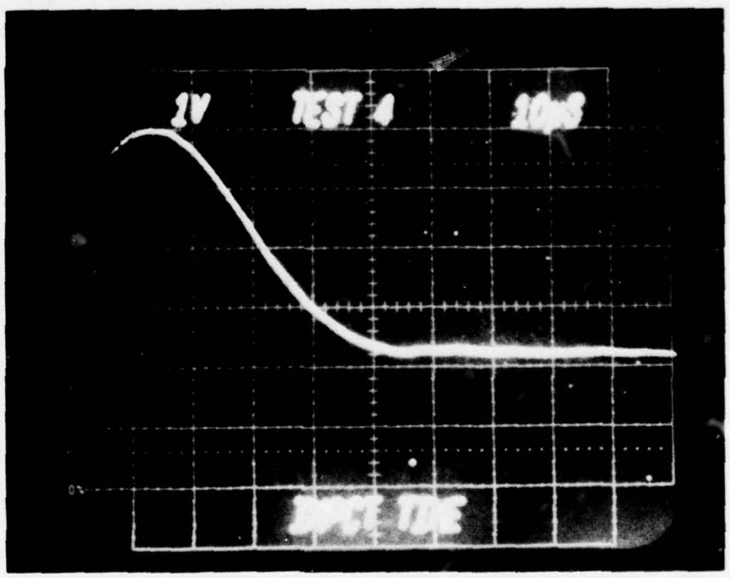

Figure 4.7 - Pressure Transducer Output at Impact Point Vs Time (Tests 3 and 4)

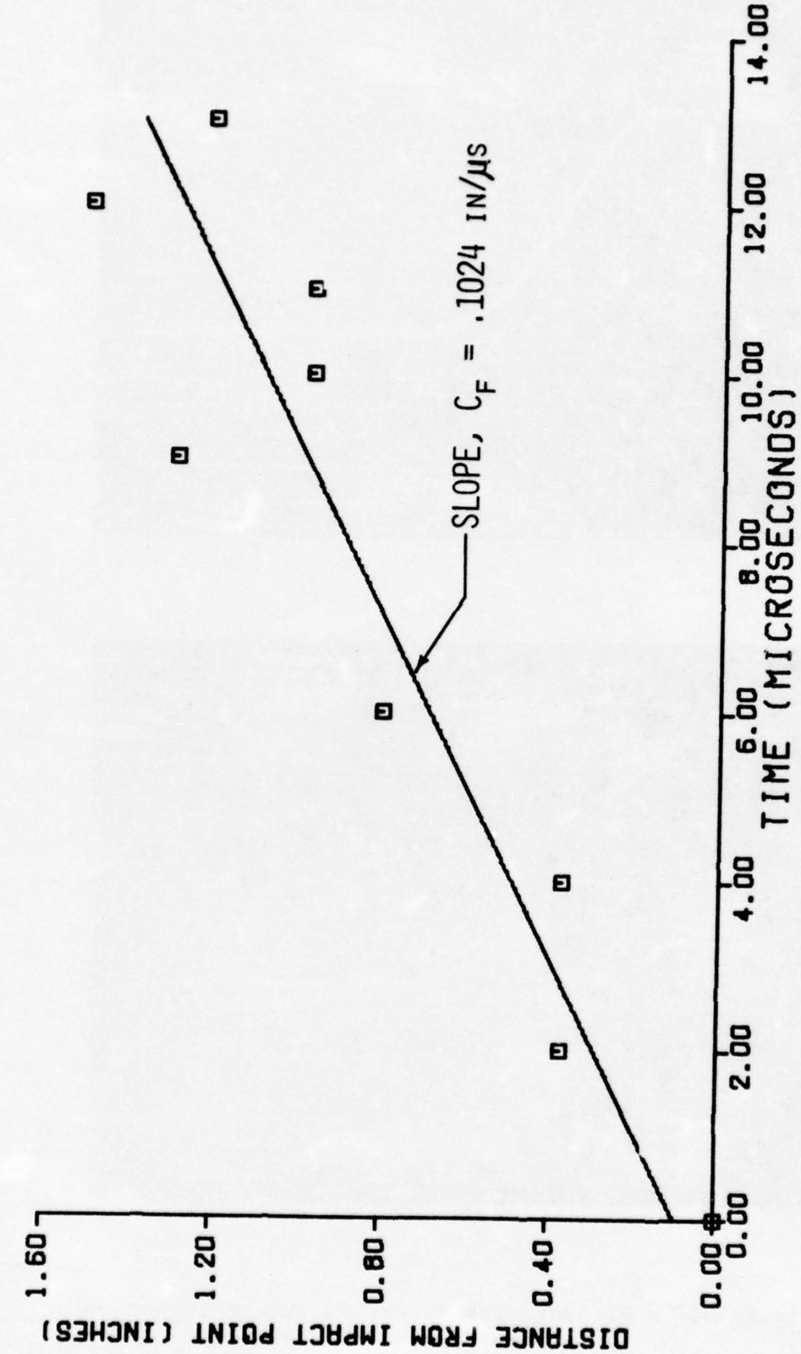

Figure 4.8 - Flexural Wave Position As a Function of Time After Impact

It is of interest to compare the experimental value of the flexural wave velocity to that obtained using the three-dimensional equations of elasticity (Ref. 2, 3, and 4). According to classical plate theory, the flexural wave velocity in an infinite plate approaches that of a Rayleigh surface wave when the wavelength, λ, becomes small compared with the plate thickness, h. In the case of the present impact tests, the steel ball made contact with the plate over a circular area of less than .03125 inches in diameter. Now, the wavelength, λ, is a function of the pulse shape and plate contact area, and if the pulse loading is broken into its Fourier components, the largest component's wavelength will be on the order of twice the diameter of the contact area. Hence, the smallest value of h/λ for the plate with h = .1875 is $h/\lambda = 3$. All other values of h/λ for the higher Fourier components will be greater than this value. For values of $h/\lambda > 3$, the flexural wave velocity in a plate closely approximates that of a Rayleigh surface wave and can be obtained from the expression (Ref. 4).

$$C_f = .932\, C_s \qquad (\nu = 1/3) \qquad (4.1)$$

where $C_s = \sqrt{\frac{G}{\rho}} = \sqrt{\frac{E}{2(1+\nu)\rho}}$ is the shear wave velocity.

For the test plate; $E = 1\text{x}10^7$ psi, $\nu = .3$, and $\rho = 2.587 \times 10^{-4}$ lbm. Placing these values into equation (4.1) yields a value of $C_f = .112$ in/μs. This is within + 8.5% of the experimental value.

The magnitude of the plate's displacement can be obtained from the fringe photographs using the expression (Ref. 5 and 6):

$$\vec{\delta}\cdot(\vec{n}_o + \vec{n}_v) = \frac{(2N\mp1)\lambda}{2}, \quad \text{for} \quad N = \pm1, \pm2, \pm3 \; . \; . \; . \; . \qquad (4.2)$$

where $\vec{\delta}$ - displacement vector

$\vec{n}_o$ - unit vector in direction from object to illumination source (object beam)

$\vec{n}_v$ - unit vector in direction from viewer (through hologram) to object

λ - wavelength of laser used to make the hologram

N - fringe order

The vectors given by equation (4.2) are shown in the context of the present experimental geometry in Figure 4.9.

Carrying out the dot product in equation (4.2) yields:

$$|\vec{\delta}|\,|\vec{n}_o + \vec{n}_v|\,\mathrm{Cos}(\vec{n}_o, \vec{n}_v) = \frac{(2N\mp1)\lambda}{2} \qquad (4.3)$$

letting $|\vec{\delta}| \equiv \delta$ and using Figure 4.9 gives

$$|\vec{n}_o + \vec{n}_v| = |\ 1.975\ \vec{i} + .222\ \vec{j}| = 1.987 \qquad (4.4)$$

$$\mathrm{Cos}\ (\vec{n}_o, \vec{n}_v) = .975 \qquad (4.5)$$

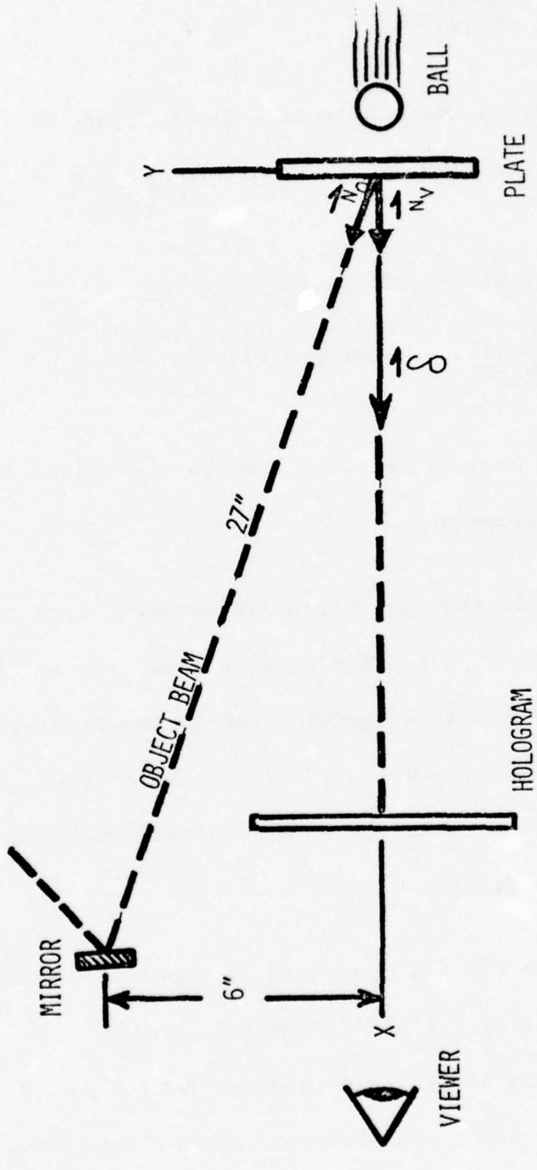

Figure 4.9 - Vector Diagram For Normal Displacement Computation

Hence, the displacement, δ, in the direction that bisects $\vec{n}_o$ and $\vec{n}_v$ is:

$$\delta = \frac{(2N \mp 1)\lambda}{(2)(.975)(1.987)} = \frac{(2N \mp 1)\lambda}{3.874} \qquad (4.6)$$

The displacement normal (perpendicular) to the plate surface differs from that given in equation (4.5) by only $\text{Cos}\left(\frac{\vec{n}_o, \vec{n}_v}{2}\right) = .994$.

Dividing equation (4.6) by .994 gives

$$\delta_n = \frac{(2N \mp 1)\lambda}{3.853}, \qquad \text{for } N = \pm 1, \pm 2, \pm 3 \ldots \qquad (4.7)$$

Equation (4.7) will be used below to compute the values of the plate's normal displacement.

Figures 4.10-4.13 show the plate displacement as a function of the distance from the impact point along a line from the impact point to the free edge of the plate (Section A-A in the figures) for times after impact of 4, 6, 12, and 18μs. Also shown in these figures are the normal displacement curves based on finite element analysis which will be discussed in Section V.

Polaroid type 55 P/N film was used to photograph the double exposure holograms using a 4"x5" format view camera with a Polaroid film holder. Polaroid 55 P/N film produces both a positive and negative print. The negative print was placed in a standard photographic enlarger such that the enlarged view of the displacement fringes could be used to more accurately determine the corresponding displacement. Using the enlarger, fringes as high as N=70 could be

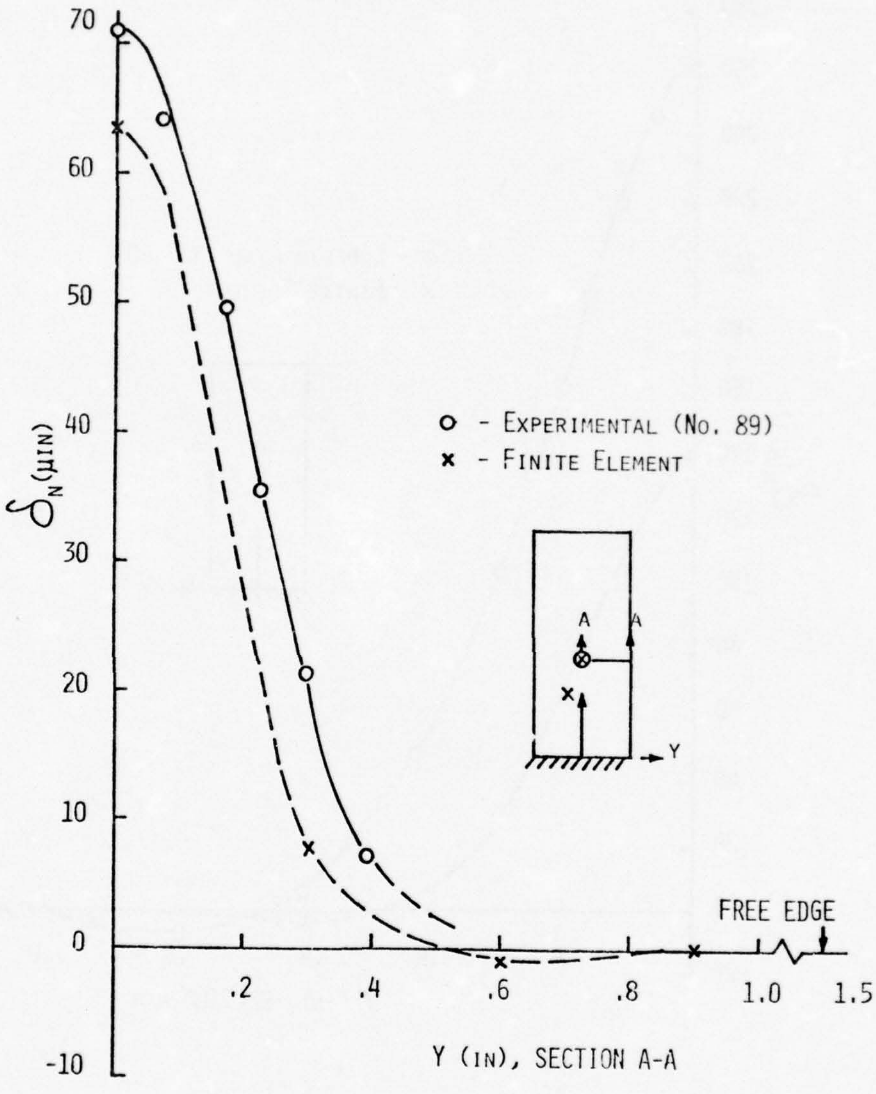

Figure 4.10 - Normal Displacement, δ_n, Vs Distance From Impact Point, Y, at T=4μs

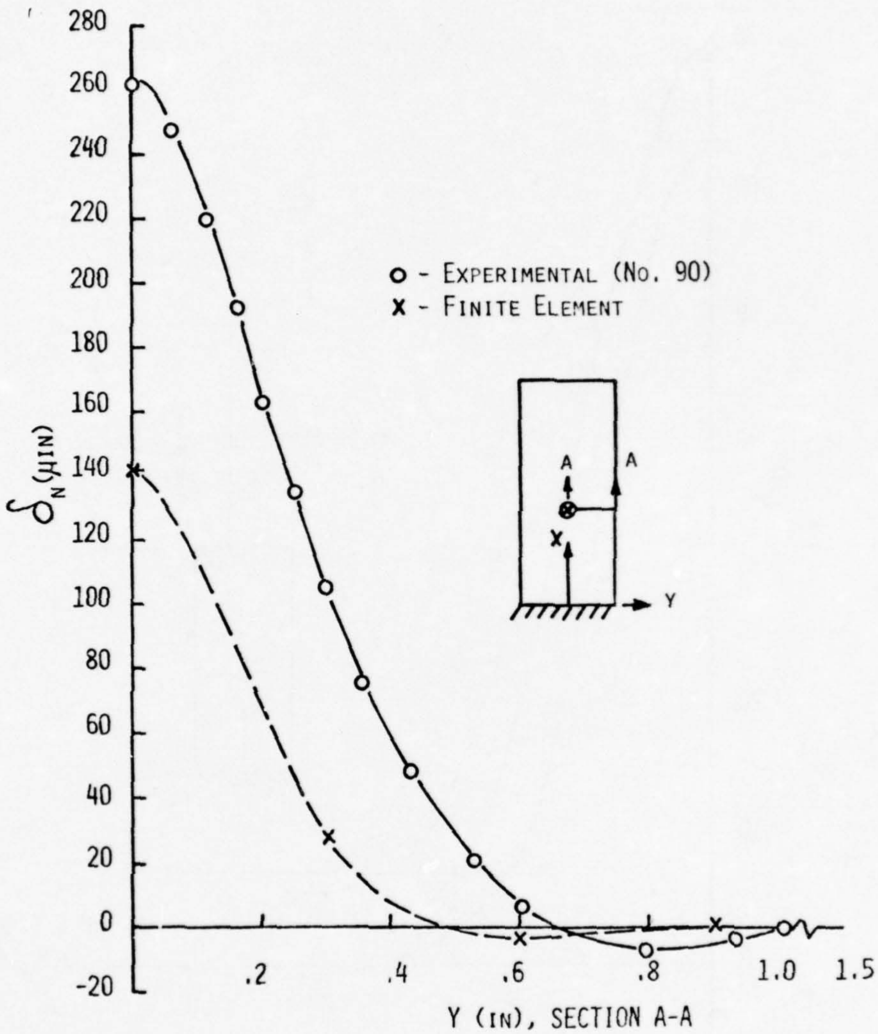

Figure 4.11 - Normal Displacement, δ_n, Vs Distance From Impact Point, Y, at T=6us

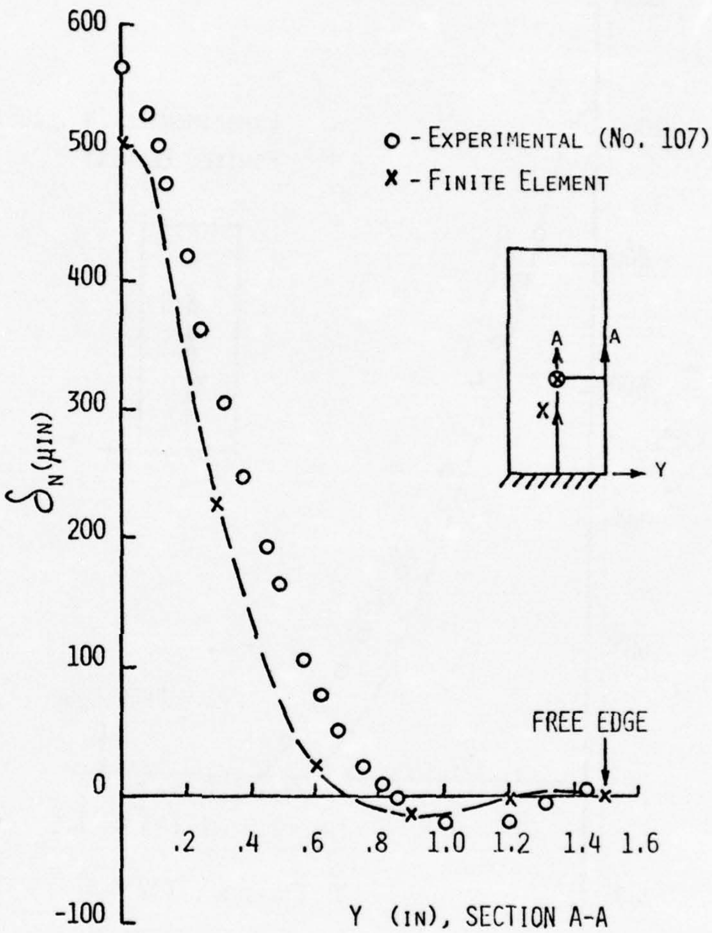

Figure 4.12 - Normal Displacement, δ_n, Vs Distance From Impact Point, Y, at T=12μs

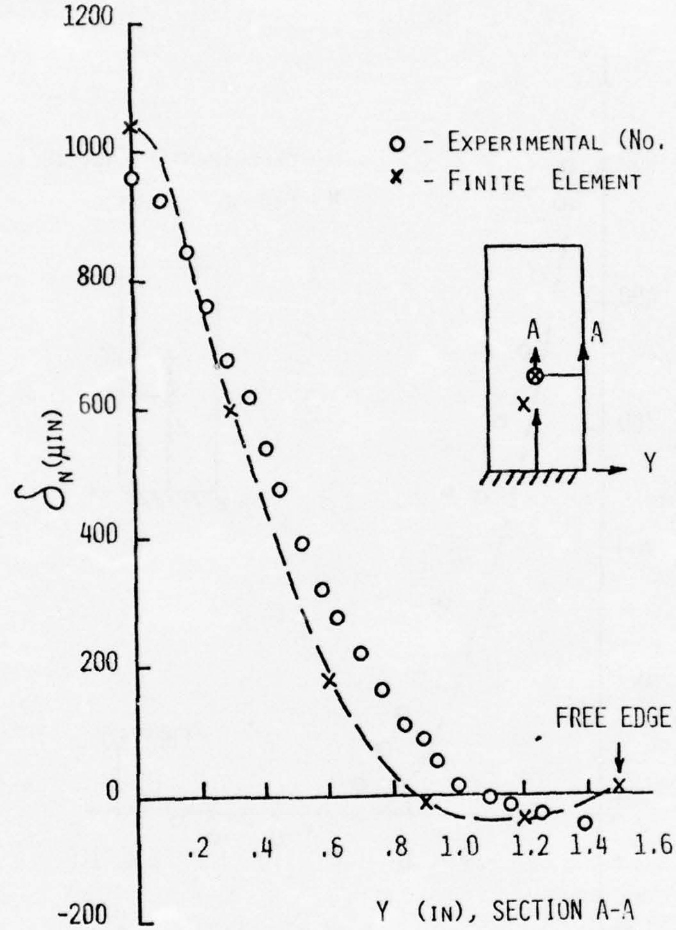

Figure 4.13 - Normal Displacement, δ_n, Vs Distance From Point, Y, at T=18μs

observed. (Note that this technique could be conveniently expanded to include a digital X-Y plotting table as the projecting surface for the enlarger.)

In contrast to time-average holography where the white fringe denoting zero displacement is the most intense and stands out clearly, the fringe representing zero displacement in double exposure holography is of the same intensity as its neighboring higher order fringes. Hence, in order to get a quantitative plot of the displacement based on a single hologram, some a priori information on the plate's displacement response is necessary. Referring to Figures 4.1, 4.2, and 4.3, the maximum plate displacement occurs at the impact point and decreases in magnitude as one travels outward from it. Since the flexural displacement is a wave, the positive displacement at the impact point will be followed by a smaller negative one at some distance from the impact point and then, as one travels further away from the impact center, a return to the undeformed, zero displacement, portion of the plate. The peak negative displacement manifests itself by a widening of the fringes where the slope of the negative displacement goes to zero. This can be seen in Figure 4.3 in the 12μs (107) photograph. Using this type of reasoning the plate's normal displacement could be plotted. While this approach was found to be sufficient for the simple deformation pattern that the plate experienced, more complex displacements would necessitate more sophisticated approaches such as multiple double exposure holograms. As an aside, another approach that could be used to determine the zero displacement fringe would be to use an optical bench telescope to scan across the image of the hologram. By scanning along a horizontal line passing through the impact point, the concentrically located fringes will appear to converge toward one of the circular fringes. In other words, the impact point will appear to be a fringe "source" with fringes traveling toward the one stationary circular fringe. Fringes located outside the stationary circular fringe will appear to travel in the direction of the impact point and the stationary circular fringe. The stationary fringe is a loci of zero displacement and by viewing the convergence (traveling) characteristics of the adjacent fringes, it can be located.

Figure 4.14 shows a plot of the plate's normal displacement along its free edge (Section B-B) at T=24μs after impact. The displacement curve is based on the third fringe photograph shown in Figure 4.14 and shown enlarged in Figure 4.15. The fringes are numbered in Figure 4.15. Along the free edge, the undeformed plate was used as the zero reference point. In addition, fringes that curved from one point on the free edge to another provided a convenient indicator of points of equal displacement on the opposite sides of a hill or a valley.

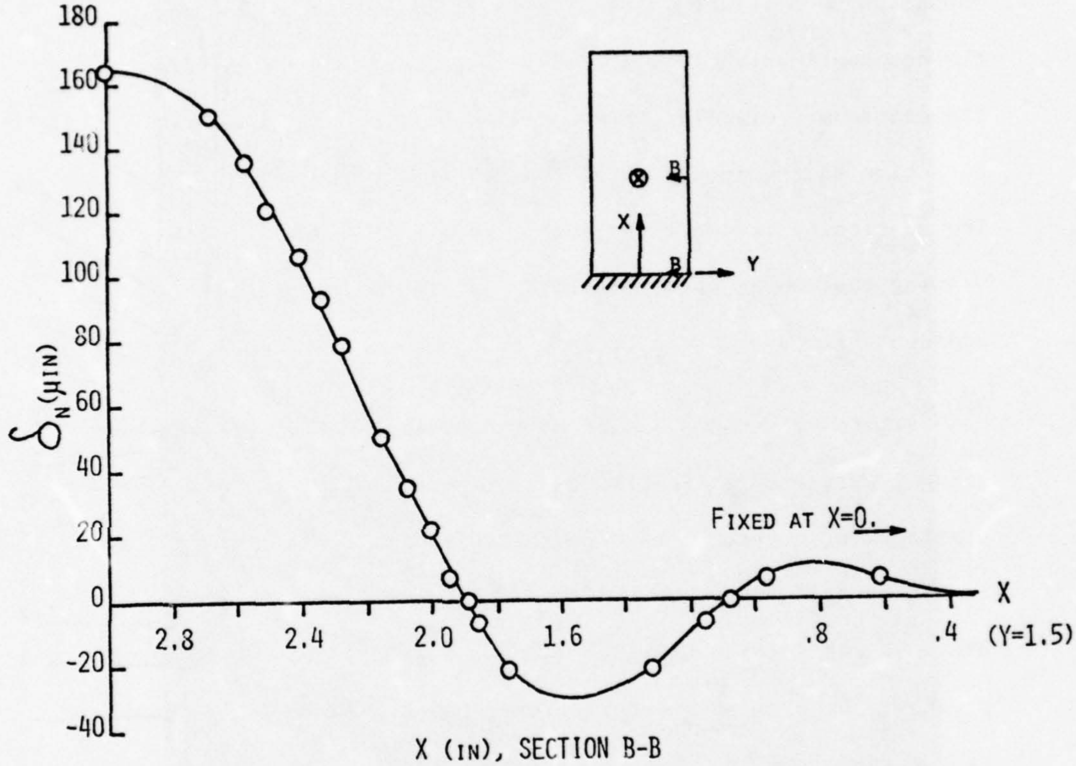

Figure 4.14 - Normal Displacement Along Plate Free Edge at T=24μs

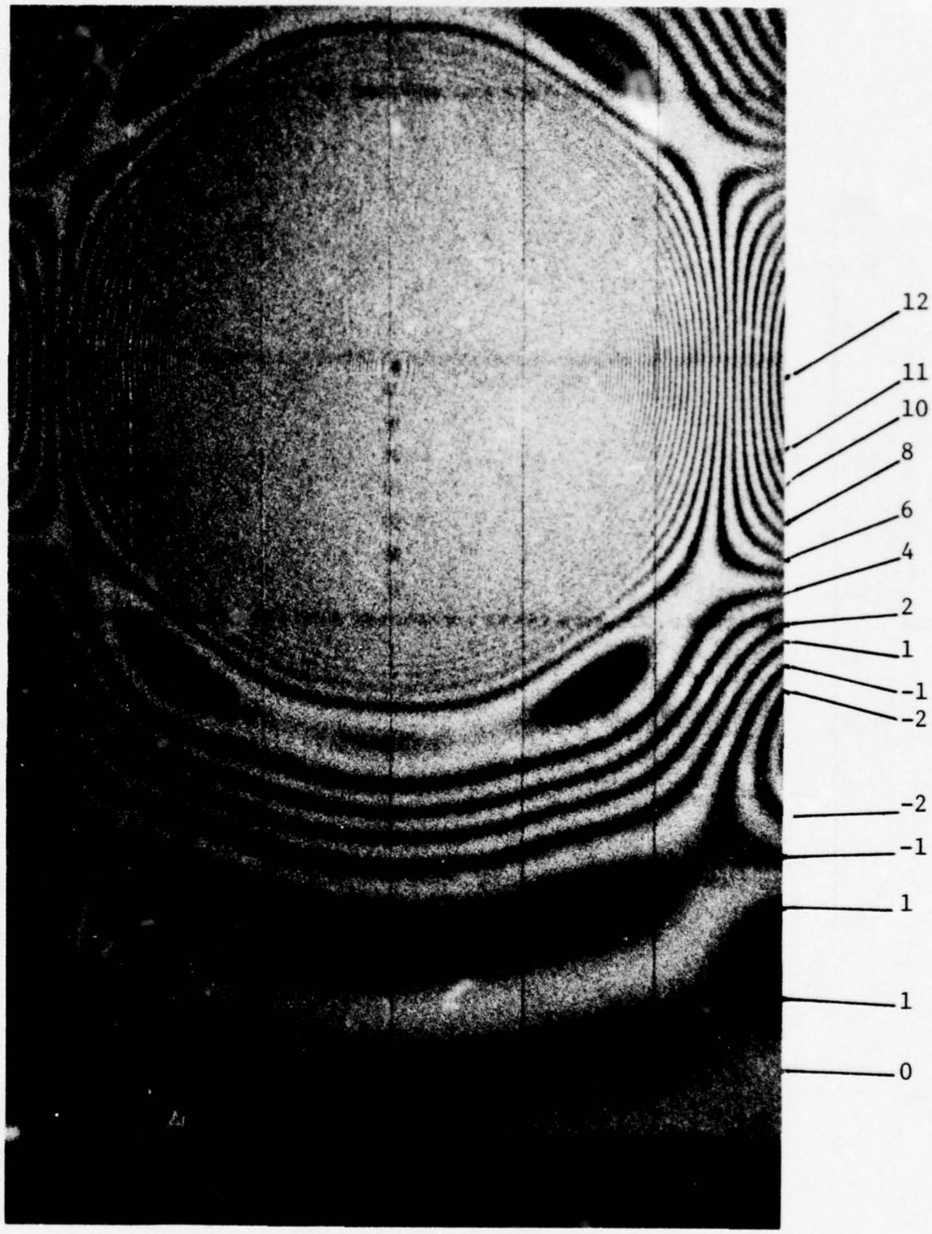

Figure 4.15 - Enlarged View of Impacted Plate at T=24μs Showing Numbered Fringes

SECTION V

FINITE ELEMENT ANALYSIS AND RESULTS

5.1 Finite Element Model

The numerical portion of the study was based on a finite element analysis of the cantilever plate using the general purpose finite element computer program, NASTRAN (Navy Nastran, Level 15.2.0). The model geometry and orientation for the cantilever plate is shown in Figure 5.1. The mesh consists of 304 nodes that connect the 165 quadrilateral plate elements (CQUAD2). The nodes at the base of the plate were fixed against both translation and rotation to simulate the cantilever condition. Because the impact load acts symmetrically with respect to the long axis of the plate, only half the plate was modelled with the nodes along the plate's axis of symmetry being fixed against asymmetrical motions, namely, translation in the Y direction and rotation about the X axis. These assumptions yield a finite element model having 957 degrees of freedom. Note that a refined mesh was used in the area about the impact point (shown by arrow). The plate response was essentially the same whether or not the refined mesh was used (thus demonstrating convergence) but better contour plots resulted when the finer mesh was used.

The transient analysis module of NASTRAN, Rigid Format 9, was used to carry out the analysis. When using the transient analysis module one can elect to use either a modal superposition technique or a direct integration of the nodal displacements. The latter

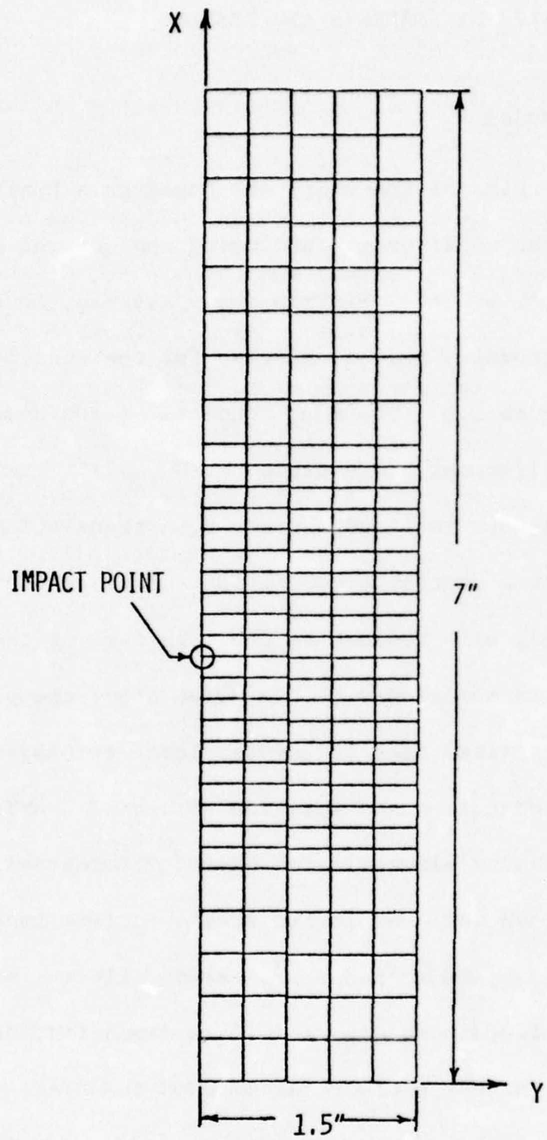

Figure 5.1 - Finite Element Mesh of Cantilever Plate

technique of direct integration was adopted for this study because it would have taken a prohibitive number of normal modes and frequencies to effectively model the plate response for an impact load that had a duration of 55μs. A good rule of thumb when using the modal superposition method is that both the integration step size and the period of the highest normal mode should be, at most, one-tenth the size of the force duration. For the present study, this would have required the highest mode of vibration to have a period of about 5μs, i.e., a natural frequency of 2×10^5 Hz. This fact, coupled with the additional fact that the direct integration technique is inherently more accurate since it handles all degrees of freedom, lead to its choice as the solution technique.

The transient analysis module of NASTRAN accepts the forcing function in tabular form where the load amplitude and direction versus time are input for each node in the area of the load. For the present study, a single load in the normal (Z) direction was input as a function of time at the node designated by the arrow in Figure 5.1 (node number 171). The load profile was assumed to be the shape of a half sine wave (see Figures 4.6 and 4.7) having a duration of 55μs. By measuring the height of the ballistic pendulum at its release point and at its maximum rebound position from the plate, the amplitude of the half sine load can be obtained by equating the maximum kinetic energy to the maximum potential energy of the pendulum. For a pendulum of mass, m, being released at height, h_1, and rebounding to a height of h_2, equating the maximum potential and kinetic energies yields a change in velocity of:

$$V_1 - V_2 = \sqrt{2g} \; (\sqrt{h_1} - \sqrt{h_2}) \tag{5.1}$$

where g is the acceleration of gravity.

The impulse of the force, F(t), acting for a time, T, is

$$I = \int_0^T F(t)dt = m \; (V_1 - V_2). \tag{5.2}$$

For a force having a half sine wave profile,

$$F(t) = A \text{ Sin} \left(\frac{\pi t}{T}\right) \tag{5.3}$$

where A is the force amplitude.

Utilizing equations (5.1) and (5.3) in equation (5.2) yields

$$I = \int_0^T A \text{ Sin} \frac{\pi t}{T} \, dt = m \sqrt{2g} \; (\sqrt{h_1} - \sqrt{h_2}) \tag{5.4}$$

Carrying out the integration and solving for the amplitude gives:

$$A = \frac{\pi m \sqrt{2g} \; (\sqrt{h_1} - \sqrt{h_2})}{2T} \tag{5.5}$$

The mass of the steel ball was 1.335×10^{-3} slugs. From Figure 3.1, it is seen that $h_1 = 9.75''$. The rebound height was measured by taking a photograph of the ball's trajectory while illuminating it with a high frequency strobe light. The height, h_2, was found to be .263". Placing these values into equation (5.5) yields an amplitude of A = 230 lbf. Hence, the force on the plate is

$$F(t) = 230 \text{ Sin} \left(\frac{\pi t}{55\mu s}\right) \qquad (5.6)$$

Equation (5.6) was used in tabular form in NASTRAN. (This is done using the "DAREA" and "TABLED1 75" bulk data cards in NASTRAN as shown in the Appendix).

5.2 Results of the Finite Element Analysis

Using the finite element mesh, boundary conditions, and impact load profile described above, NASTRAN computed the plate displacement for specified times after impact. The output was in the form of displacements at specified nodes plus contour plots of the displacement for the entire plate. The normal plate displacement was plotted as a function of the distance (Y) from the impact point at X=3" for times after impact of 4, 6, 12, and 18μs. For purposes of comparison with the experimental results, the four plots are shown in Figures 4.10 through 4.13 of Section IV as the dashed curves. The agreement between the experimental and finite element result is quite good except for T=6μs. This is felt to be due to a stronger than average impact load for the experimental curve. This agreement is corroborated by a look at Figure 5.2 where the displacement of the plate impact point is shown plotted as a function of time. A computer generated second order least squares curve fit the finite element data exactly, demonstrating a parabolic relationship between the impact point dis-

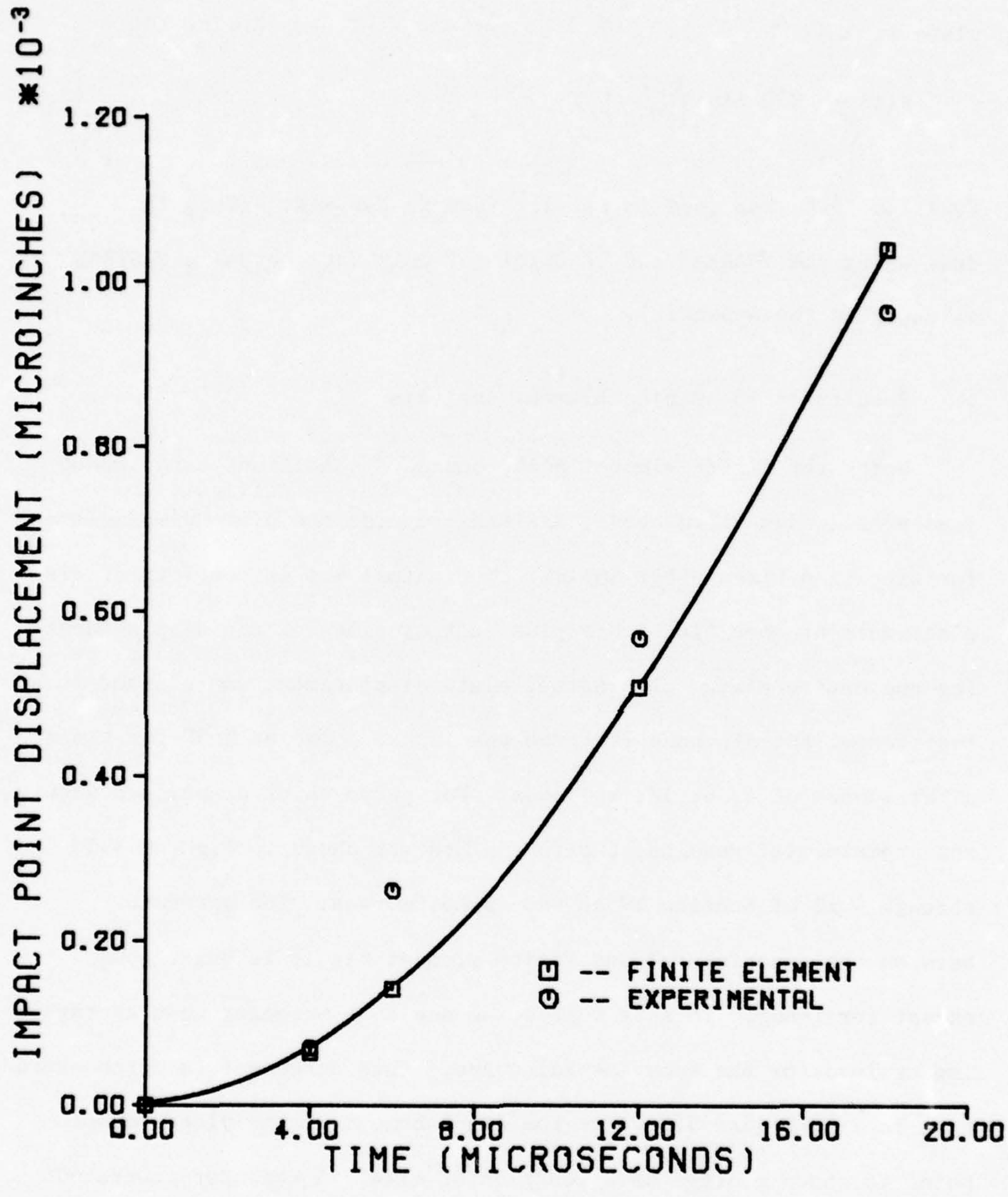

Figure 5.2 - Impact Point Displacement Vs Time

placement and time. The experimentally derived points closely follow this curve with the displacement at T=6μs showing the largest deviation, as one would expect.

Figures 5.3 through 5.5 show normal displacement contours of the plate response at times after impact of 6, 8, 12, 18, 24, and 30μs. The values of the contours are given in Table 5.1. The trends demonstrated by the contour plots are in good agreement with the experimental results. Note in Figure 5.5 that reflection has started to take place off the free edge for T=30μs. While some of the symbols in the contour plots may be difficult to discern, the reader can be aided by the fact that contour numbers 1 through 29 represent increasing positive displacement and numbers 30 through 50 represent increasing negative displacement. This means that a loci of zero displacement lies between contours 1 and 31, exclusive.

TABLE 5.1

Normal Displacement Magnitude for NASTRAN Contour Plots (See Figures 5.3 - 5.5)

SYMBOL	DISPLACEMENT (IN.)	SYMBOL	DISPLACEMENT (IN.)
1	1.00E-05	26	9.00E-04
2	2.00E-05	27	9.50E-04
3	3.00E-05	28	1.00E-03
4	4.00E-05	29	1.05E-03
5	5.00E-05	30	-1.00E-05
6	6.00E-05	31	-2.00E-05
7	7.00E-05	32	-3.00E-05
8	8.00E-05	33	-4.00E-05
9	9.00E-05	34	-5.00E-05
10	1.00E-04	35	-6.00E-05
11	1.50E-04	36	-7.00E-05
12	2.00E-04	37	-8.00E-05
13	2.50E-04	38	-9.00E-05
14	3.00E-04	39	-1.00E-04
15	3.50E-04	40	-1.50E-04
16	4.00E-04	41	-2.00E-04
17	4.50E-04	42	-2.50E-04
18	5.00E-04	43	-3.00E-04
19	5.50E-04	44	-3.50E-04
20	6.00E-04	45	-4.00E-04
21	6.50E-04	46	-4.50E-04
22	7.00E-04	47	-5.00E-04
23	7.50E-04	48	-5.50E-04
24	8.00F-04	49	-6.00E-04
25	8.50E-04	50	-6.50E-04

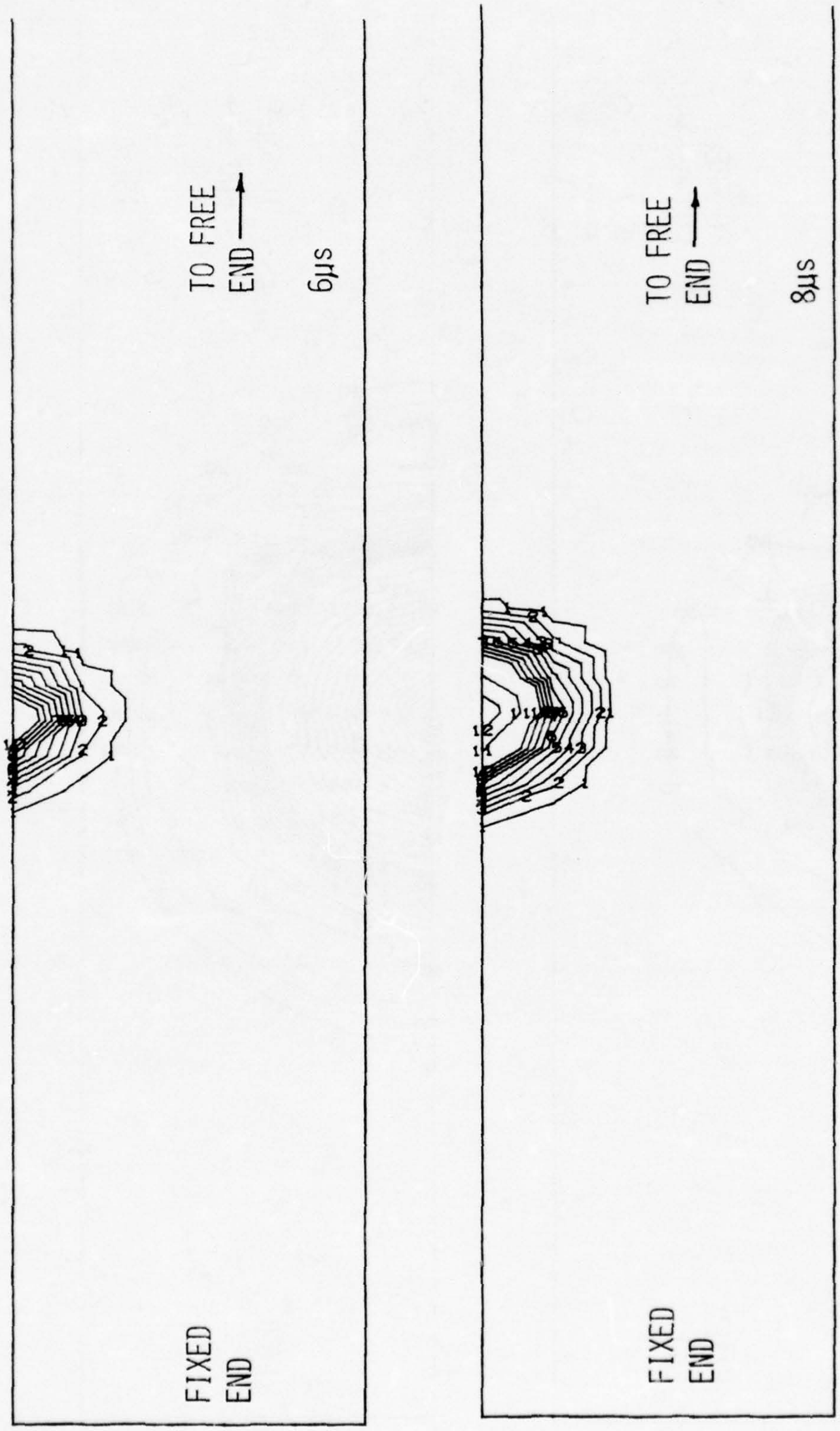

Figure 5.3 - NASTRAN Contour Plot of Normal Displacement at T=6μs and T=8μs

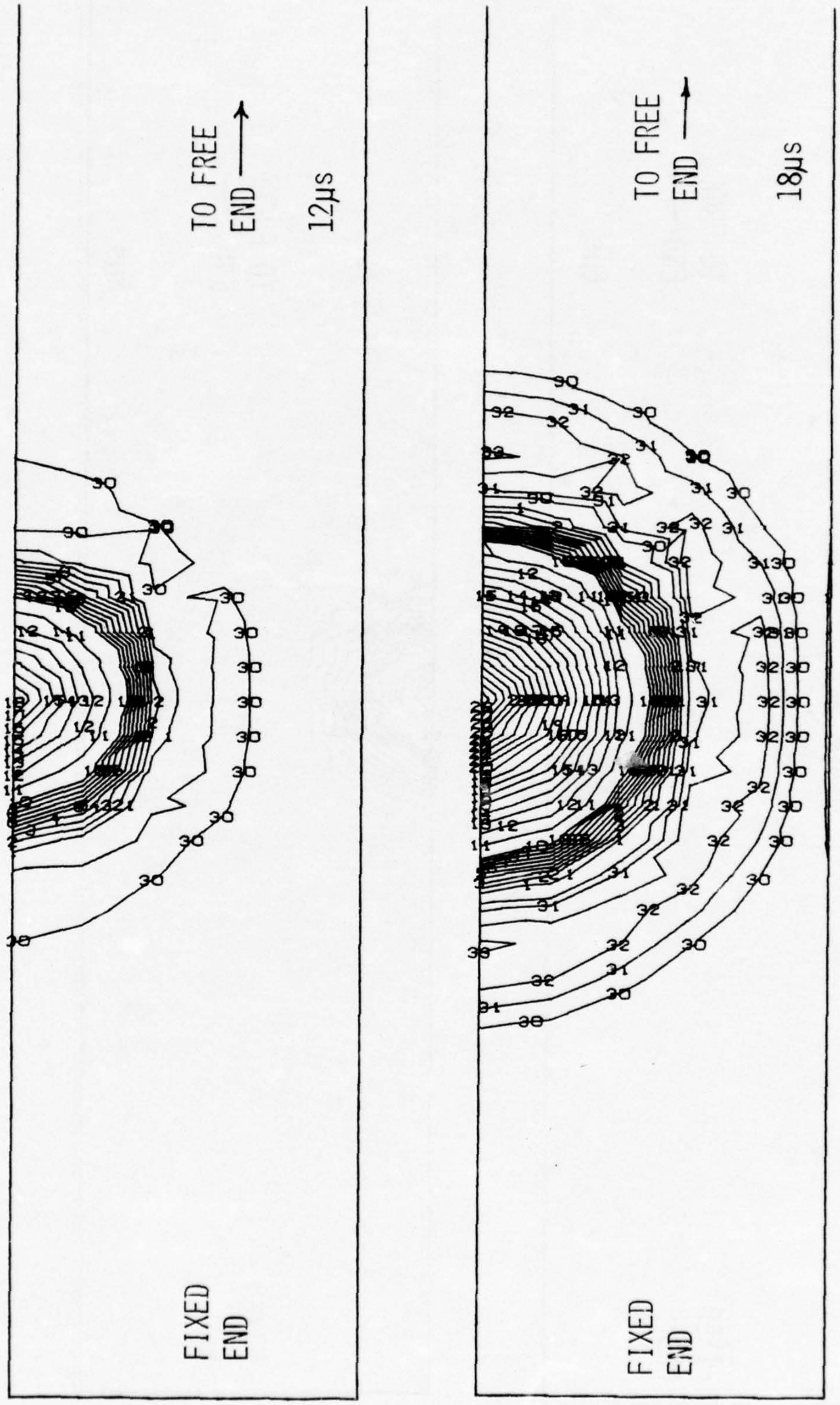

Figure 5.4 - NASTRAN Contour Plot of Normal Displacement at T=12μs and T=18μs

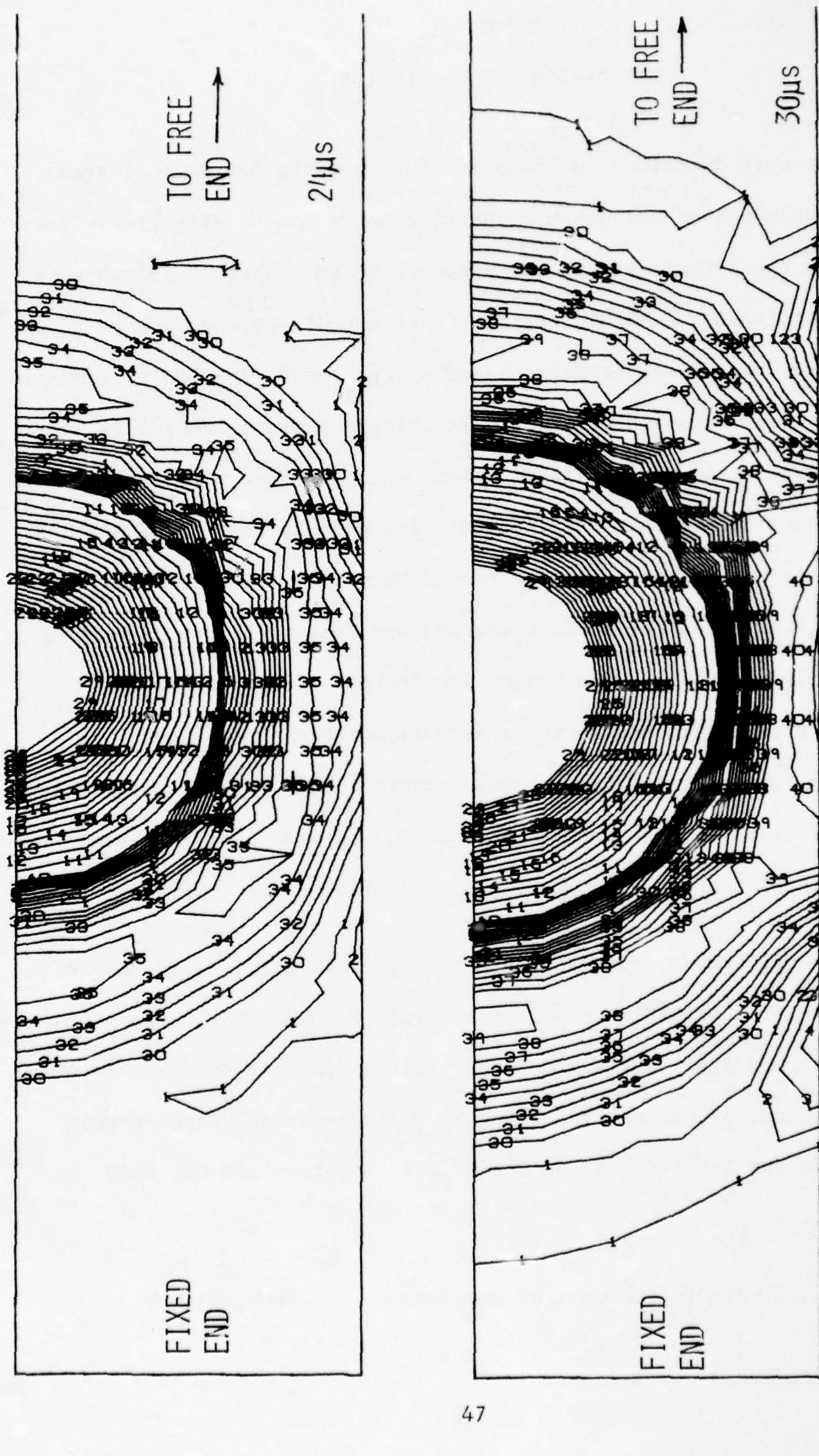

Figure 5.5 - NASTRAN Contour Plot of Normal Displacement at T=24μs and T=30μs

SECTION VI

DISCUSSION AND CONCLUSION

The work described in the preceding sections has demonstrated that double pulsed holographic interferometry can be effectively used to study the dynamic structural response of an elastic body subjected to impact loading. Within the limits of the displacement range covered by pulsed laser interferometry using a ruby laser (5-1000μin), quantitative displacement information describing a plate's initial response to an impact load was obtained. There was good agreement between the experimental tests and analytical results obtained using the NASTRAN finite element computer program (Rigid Format 9). Some scatter between individual tests did occur and was felt to be due to failure to accurately reproduce the impact load on the plate. Future work in this area should strive for a more repeatable impact load. In addition, experimental timing measurements should be increased to a sensitivity of ±0.1 μs instead of the ±0.5 μs used in the present experimental tests.

The good experimental/analytical agreement provides increased confidence in NASTRAN's transient analysis module. The good agreement does not come free, however. For a typical computer run (see Appendix), central processor (CP) time was 923 seconds and input/output (IO) time was 1360 seconds on the Wright-Patterson AFB CDC 6600 Computer.

Future work in the vein of the current research will use the existing system to study turbine fan blade response to impact load. Some thought is also being given to utilizing the measurement of the plate flexural wave speed to determine elastic material properties of composites (say) and, also, to study material damping characteristics. Finally, plate displacements, at times greater than those dealt with in this report (2-30μs), could be studied using the double-pulse capability of AFAPL's ruby laser.

REFERENCES

1. Collier, R.J., Burckhardt, C.B.; and Lin, L.H.; Optical Holography, Academic Press, New York, 1971.

2. Lamb, H., "On Waves in an Elastic Plate", Proceedings of the Royal Society of London, England, Series A, Vol. 93, 1917, pp 114-128.

3. Kolsky, H., Stress Waves in Solids, Dover Publications, Inc. New York, 1963, pp 16-23.

4. Mindlin, R.D., "Influence of Rotatory Inertia and Shear on Flexural Motions of Isotropic Elastic Plates", J. of Applied Mechanics, Vol. 18, No. 1, Mar, 1951, pp 31-38.

5. Aleksandrov, E.B. and Bonch-Bruevich, A.M., "Investigation of Surface Strains by the Hologram Technique", Soviet Physics, Technical Physics (ZTF), Vol. 12, No. 2, August, 1967, pp 258-265.

6. Haines, K.A., and Hildebrand, B.P., "Surface Deformation Measurement Using the Wavefront Reconstruction Technique", Applied Optics, Vol. 5, No. 4, April 1966, pp 595-602.

APPENDIX

NASTRAN Program Listing

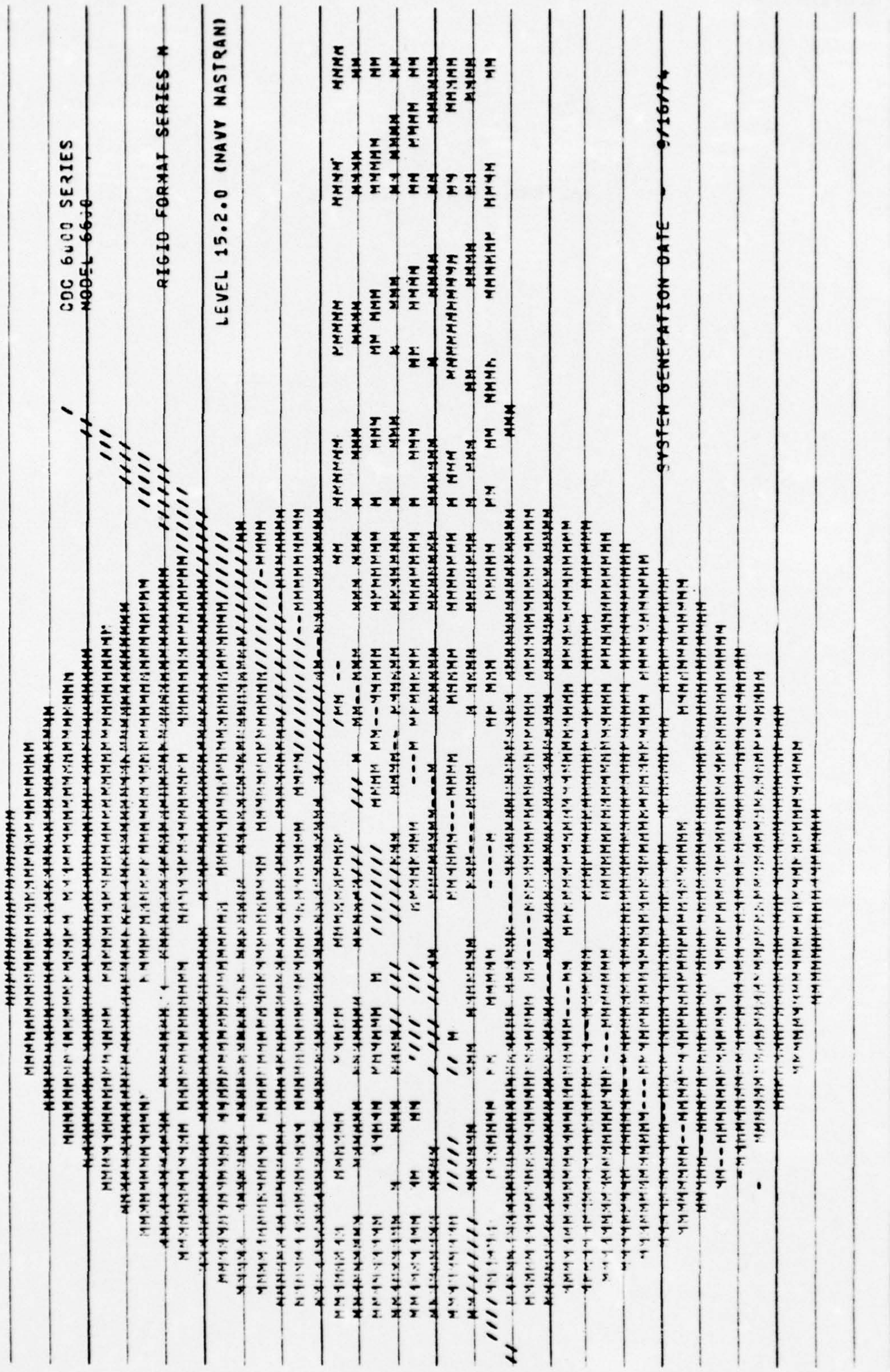
CDC 6000 SERIES
MODEL 66.0
RIGID FORMAT SERIES M
LEVEL 15.2.0 (NAVY NASTRAN)
SYSTEM GENERATION DATE - 9/16/74

N A S T R A N   E X E C U T I V E   C O N T R O L   D E C K   E C H O

```
ID TWISTED PLATE - NASTRAN
DIAG 14
TIME 40
CHKPNT YES
APP DISP
SOL 9,0
CEND
```

```
        N A S T R A N   E X E C U T I V E   C O N T R O L   D E C K   E C H O

ECHO OF FIRST CARD IN CHECKPOINT DICTIONARY TO BE PUNCHED OUT FOR THIS PROBLEM
   RESTART   TWISTED ,PLATE    , 7/ 2/76,   10042,
```

```
PLATE TRANSIENT RESPONSE
                    C A S E   C O N T R O L   D E C K   E C H O
  CARD
  COUNT
    1      TITLE= PLATE TRANSIENT RESPONSE
    2      SPC=2
    3      TSTEP=60
    4      SET 2=176,165,154,143,132,121,110,99,88,77,66,55,44,33,22,11
    5        METHOD= 1
    6      SUBCASE 1
    7      SUBTITLE=HALF SINE LOAD
    8      DLOAD=70
    9      DISP=2
   10      PLOTID= FLAT PLATE / FINITE ELEMENT
   11      OUTPUT(PLOT)
   12      PLOTTER CALCOMP , MODEL 765,105
   13      SET 1= QUAD2
   14      VIEW 90.,.,89.
   15      SCALE 1.5
   16      MAXIMUM DEFORMATION .1
   17      FIND      ORIGIN 1,SET 1
   18      CONTOUR ZDISP LIST .00001,.00002,.00003,.00004,.00005,.00006,.00007,
   19              .00008,.00009,.0001,.00015,.0002,.00025,.0003,.00035,.0004,.00045,
   20              .0005,.00055,.0006,.00065,.0007,.00075,.0008,.00085,
   21              .0009,.00095,.001,.00105,
   22              -.00001,-.00002,-.00003,-.00004,-.00005,-.00006,-.00007,
   23              -.00008,-.00009,-.0001,-.00015,-.0002,-.00025,-.0003,-.00035,
   24              -.0004,-.00045,-.0005,-.00055,-.0006,-.00065
   25      PLOT TRANSIENT DEFORMATION CONTOUR 1,TIME 1.90-6,2.10-6,SET 1,SYMBOL 0,
   26       OUTLINE
   27      CONTOUR ZDISP LIST .00001,.00002,.00003,.00004,.00005,.00006,.00007,
   28              .00008,.00009,.0001,.00015,.0002,.00025,.0003,.00035,.0004,.00045,
   29              .0005,.00055,.0006,.00065,.0007,.00075,.0008,.00085,
   30              .0009,.00095,.001,.00105,
   31              -.00001,-.00002,-.00003,-.00004,-.00005,-.00006,-.00007,
   32              -.00008,-.00009,-.0001,-.00015,-.0002,-.00025,-.0003,-.00035,
   33              -.0004,-.00045,-.0005,-.00055,-.0006,-.00065
   34      PLOT TRANSIENT DEFORMATION CONTOUR 1,TIME 3.90-6,4.10-6,SET 1,SYMBOL 0,
   35       OUTLINE
   36      CONTOUR ZDISP LIST .00001,.00002,.00003,.00004,.00005,.00006,.00007,
   37              .00008,.00009,.0001,.00015,.0002,.00025,.0003,.00035,.0004,.00045,
   38              .0005,.00055,.0006,.00065,.0007,.00075,.0008,.00085,
   39              .0009,.00095,.001,.00105,
   40              -.00001,-.00002,-.00003,-.00004,-.00005,-.00006,-.00007,
   41              -.00008,-.00009,-.0001,-.00015,-.0002,-.00025,-.0003,-.00035,
   42              -.0004,-.00045,-.0005,-.00055,-.0006,-.00065
   43      PLOT TRANSIENT DEFORMATION CONTOUR 1,TIME 5.90-6,6.10-6,SET 1,SYMBOL 0,
   44       OUTLINE
   45      CONTOUR ZDISP LIST .00001,.00002,.00003,.00004,.00005,.00006,.00007,
   46              .00008,.00009,.0001,.00015,.0002,.00025,.0003,.00035,.0004,.00045,
   47              .0005,.00055,.0006,.00065,.0007,.00075,.0008,.00085,
   48              .0009,.00095,.001,.00105,
   49              -.00001,-.00002,-.00003,-.00004,-.00005,-.00006,-.00007,
   50              -.00008,-.00009,-.0001,-.00015,-.0002,-.00025,-.0003,-.00035,
```

```
PLATE TRANSIENT RESPONSE
                        C A S E   C O N T R O L   D E C K   E C H O
    CARD
    COUNT
     51            -.0004,-.00045,-.0005,-.00055,-.0006,-.00065
     52      PLOT TRANSIENT DEFORMATION CONTOUR 1,TIME 7.90-6,8.10-6,SET 1,SYMBOL 0,
     53       OUTLINE
     54      CONTOUR ZDISP LIST .00001,.00002,.00003,.00004,.00005,.00006,.00007,
     55            .00008,.00009,.0001,.00015,.0002,.00025,.0003,.00035,.0004,.00045,
     56            .0005,.00055,.0006,.00065,.0007,.00075,.0008,.00085,
     57            .0009,.00095,.001,.00105,
     58            -.00001,-.00002,-.00003,-.00004,-.00005,-.00006,-.00007,
     59            -.00008,-.00009,-.0001,-.00015,-.0002,-.00025,-.0003,-.00035,
     60             -.0004,-.00045,-.0005,-.00055,-.0006,-.00065
     61      PLOT TRANSIENT DEFORMATION CONTOUR 1,TIME 11.9-6,12.1-6,SET 1,SYMBOL 0,
     62       OUTLINE
     63      CONTOUR ZDISP LIST .00001,.00002,.00003,.00004,.00005,.00006,.00007,
     64            .00008,.00009,.0001,.00015,.0002,.00025,.0003,.00035,.0004,.00045,
     65            .0005,.00055,.0006,.00065,.0007,.00075,.0008,.00085,
     66            .0009,.00095,.001,.00105,
     67            -.00001,-.00002,-.00003,-.00004,-.00005,-.00006,-.00007,
     68            -.00008,-.00009,-.0001,-.00015,-.0002,-.00025,-.0003,-.00035,
     69             -.0004,-.00045,-.0005,-.00055,-.0006,-.00065
     70      PLOT TRANSIENT DEFORMATION CONTOUR 1,TIME 17.9-6,18.1-6,SET 1,SYMBOL 0,
     71       OUTLINE
     72      CONTOUR ZDISP LIST .00001,.00002,.00003,.00004,.00005,.00006,.00007,
     73            .00008,.00009,.0001,.00015,.0002,.00025,.0003,.00035,.0004,.00045,
     74            .0005,.00055,.0006,.00065,.0007,.00075,.0008,.00085,
     75            .0009,.00095,.001,.00105,
     76            -.00001,-.00002,-.00003,-.00004,-.00005,-.00006,-.00007,
     77            -.00008,-.00009,-.0001,-.00015,-.0002,-.00025,-.0003,-.00035,
     78             -.0004,-.00045,-.0005,-.00055,-.0006,-.00065
     79      PLOT TRANSIENT DEFORMATION CONTOUR 1,TIME 23.9-6,24.1-6,SET 1,SYMBOL 0,
     80       OUTLINE
     81      CONTOUR ZDISP LIST .00001,.00002,.00003,.00004,.00005,.00006,.00007,
     82            .00008,.00009,.0001,.00015,.0002,.00025,.0003,.00035,.0004,.00045,
     83            .0005,.00055,.0006,.00065,.0007,.00075,.0008,.00085,
     84            .0009,.00095,.001,.00105,
     85            -.00001,-.00002,-.00003,-.00004,-.00005,-.00006,-.00007,
     86            -.00008,-.00009,-.0001,-.00015,-.0002,-.00025,-.0003,-.00035,
     87            -.0004,-.00045,-.0005,-.00055,-.0006,-.00065
     88      PLOT TRANSIENT DEFORMATION CONTOUR 1,TIME 29.9-6,30.1-6,SET 1,SYMBOL 0,
     89       OUTLINE
     90      BEGIN BULK

 *** USER INFORMATION MESSAGE 207, BULK DATA NOT SORTED,XSORT WILL RE-ORDER DECK.
```

PLATE TRANSIENT RESPONSE

SORTED BULK DATA ECHO

CARD COUNT	. 1 ..		2 ..	3 ..	4 ..	5 ..	6 ..	7 ..	8 ..	9 ..	10
1-	CQUAD2	6	1	6	17	18	7				
2-	CQUAD2	7	1	7	18	19	8				
3-	CQUAD2	8	1	8	19	20	9				
4-	CQUAD2	9	1	9	20	21	10				
5-	CQUAD2	10	1	10	21	22	11				
6-	CQUAD2	16	1	17	28	29	18				
7-	CQUAD2	17	1	18	29	30	19				
8-	CQUAD2	18	1	19	30	31	20				
9-	CQUAD2	19	1	20	31	32	21				
10-	CQUAD2	20	1	21	32	33	22				
11-	CQUAD2	26	1	28	39	40	29				
12-	CQUAD2	27	1	29	40	41	30				
13-	CQUAD2	28	1	30	41	42	31				
14-	CQUAD2	29	1	31	42	43	32				
15-	CQUAD2	30	1	32	43	44	33				
16-	CQUAD2	36	1	39	50	51	40				
17-	CQUAD2	37	1	40	51	52	41				
18-	CQUAD2	38	1	41	52	53	42				
19-	CQUAD2	39	1	42	53	54	43				
20-	CQUAD2	40	1	43	54	55	44				
21-	CQUAD2	46	1	50	61	62	51				
22-	CQUAD2	47	1	51	62	63	52				
23-	CQUAD2	48	1	52	63	64	53				
24-	CQUAD2	49	1	53	64	65	54				
25-	CQUAD2	50	1	54	65	66	55				
26-	CQUAD2	56	1	61	72	73	62				
27-	CQUAD2	57	1	62	73	74	63				
28-	CQUAD2	58	1	63	74	75	64				
29-	CQUAD2	59	1	64	75	76	65				
30-	CQUAD2	60	1	65	76	77	66				
31-	CQUAD2	66	1	72	83	84	73				
32-	CQUAD2	67	1	73	84	85	74				
33-	CQUAD2	68	1	74	85	86	75				
34-	CQUAD2	69	1	75	86	87	76				
35-	CQUAD2	70	1	76	87	88	77				
36-	CQUAD2	76	1	83	94	95	84				
37-	CQUAD2	77	1	84	95	96	85				
38-	CQUAD2	78	1	85	96	97	86				
39-	CQUAD2	79	1	86	97	98	87				
40-	CQUAD2	80	1	87	98	99	88				
41-	CQUAD2	86	1	94	105	106	95				
42-	CQUAD2	87	1	95	106	107	96				
43-	CQUAD2	88	1	96	107	108	97				
44-	CQUAD2	89	1	97	108	109	98				
45-	CQUAD2	90	1	98	109	110	99				
46-	CQUAD2	96	1	105	116	117	106				
47-	CQUAD2	97	1	106	117	118	107				
48-	CQUAD2	98	1	107	118	119	108				
49-	CQUAD2	99	1	108	119	120	109				
50-	CQUAD2	100	1	109	120	121	110				

PLATE TRANSIENT RESPONSE

SORTED BULK DATA ECHO

CARD COUNT	. 1 ..	2 ..	3 ..	4 ..	5 ..	6 ..	7 ..	8 .. 9 .. 10 .
51-	CQUAD2	106	1	116	127	128	117
52-	CQUAD2	107	1	117	128	129	118
53-	CQUAD2	108	1	118	129	130	119
54-	CQUAD2	109	1	119	130	131	120
55-	CQUAD2	110	1	120	131	132	121
56-	CQUAD2	116	1	127	138	139	128
57-	CQUAD2	117	1	128	139	140	129
58-	CQUAD2	118	1	129	140	141	130
59-	CQUAD2	119	1	130	141	142	131
60-	CQUAD2	120	1	131	142	143	132
61-	CQUAD2	126	1	138	149	150	139
62-	CQUAD2	127	1	139	150	151	140
63-	CQUAD2	128	1	140	151	152	141
64-	CQUAD2	129	1	141	152	153	142
65-	CQUAD2	130	1	142	153	154	143
66-	CQUAD2	136	1	149	160	161	150
67-	CQUAD2	137	1	150	161	162	151
68-	CQUAD2	138	1	151	162	163	152
69-	CQUAD2	139	1	152	163	164	153
70-	CQUAD2	140	1	153	164	165	154
71-	CQUAD2	146	1	160	171	172	161
72-	CQUAD2	147	1	161	172	173	162
73-	CQUAD2	148	1	162	173	174	163
74-	CQUAD2	149	1	163	174	175	164
75-	CQUAD2	150	1	164	175	176	165
76-	CQUAD2	156	1	171	182	183	172
77-	CQUAD2	157	1	172	183	184	173
78-	CQUAD2	158	1	173	184	185	174
79-	CQUAD2	159	1	174	185	186	175
80-	CQUAD2	160	1	175	186	187	176
81-	CQUAD2	166	1	182	193	194	183
82-	CQUAD2	167	1	183	194	195	184
83-	CQUAD2	168	1	184	195	196	185
84-	CQUAD2	169	1	185	196	197	186
85-	CQUAD2	170	1	186	197	198	187
86-	CQUAD2	176	1	193	204	205	194
87-	CQUAD2	177	1	194	205	206	195
88-	CQUAD2	178	1	195	206	207	195
89-	CQUAD2	179	1	196	207	208	197
90-	CQUAD2	180	1	197	208	209	198
91-	CQUAD2	186	1	204	215	216	205
92-	CQUAD2	187	1	205	216	217	206
93-	CQUAD2	188	1	206	217	218	207
94-	CQUAD2	189	1	207	218	219	208
95-	CQUAD2	190	1	208	219	220	209
96-	CQUAD2	196	1	215	226	227	216
97-	CQUAD2	197	1	216	227	228	217
98-	CQUAD2	198	1	217	228	229	218
99-	CQUAD2	199	1	218	229	230	219
100-	CQUAD2	200	1	219	230	231	220

PLATE TRANSIENT RESPONSE

SORTED BULK DATA ECHO

CARD COUNT	. 1 ..	2 ..	3 ..	4 ..	5 ..	6 ..	7 ..	8 ..	9 ..	10 .
101-	CQUAD2	206	1	226	237	238	227			
102-	CQUAD2	207	1	227	238	239	228			
103-	CQUAD2	208	1	228	239	240	229			
104-	CQUAD2	209	1	229	240	241	230			
105-	CQUAD2	210	1	230	241	242	231			
106-	CQUAD2	216	1	237	248	249	238			
107-	CQUAD2	217	1	238	249	250	239			
108-	CQUAD2	218	1	239	250	251	240			
109-	CQUAD2	219	1	240	251	252	241			
110-	CQUAD2	220	1	241	252	253	242			
111-	CQUAD2	226	1	248	259	260	249			
112-	CQUAD2	227	1	249	260	261	250			
113-	CQUAD2	228	1	250	261	262	251			
114-	CQUAD2	229	1	251	262	263	252			
115-	CQUAD2	230	1	252	263	264	253			
116-	CQUAD2	236	1	259	270	271	260			
117-	CQUAD2	237	1	260	271	272	261			
118-	CQUAD2	238	1	261	272	273	262			
119-	CQUAD2	239	1	262	273	274	263			
120-	CQUAD2	240	1	263	274	275	264			
121-	CQUAD2	246	1	270	281	282	271			
122-	CQUAD2	247	1	271	282	283	272			
123-	CQUAD2	248	1	272	283	284	273			
124-	CQUAD2	249	1	273	284	285	274			
125-	CQUAD2	250	1	274	285	286	275			
126-	CQUAD2	256	1	281	292	293	282			
127-	CQUAD2	257	1	282	293	294	283			
128-	CQUAD2	258	1	283	294	295	284			
129-	CQUAD2	259	1	284	295	296	285			
130-	CQUAD2	260	1	285	296	297	286			
131-	CQUAD2	266	1	292	303	304	293			
132-	CQUAD2	267	1	293	304	305	294			
133-	CQUAD2	268	1	294	305	306	295			
134-	CQUAD2	269	1	295	306	307	296			
135-	CQUAD2	270	1	296	307	308	297			
136-	CQUAD2	276	1	303	314	315	304			
137-	CQUAD2	277	1	304	315	316	305			
138-	CQUAD2	278	1	305	316	317	306			
139-	CQUAD2	279	1	306	317	318	307			
140-	CQUAD2	280	1	307	318	319	308			
141-	CQUAD2	286	1	314	325	326	315			
142-	CQUAD2	287	1	315	326	327	316			
143-	CQUAD2	288	1	316	327	328	317			
144-	CQUAD2	289	1	317	328	329	318			
145-	CQUAD2	290	1	318	329	330	319			
146-	CQUAD2	296	1	325	336	337	326			
147-	CQUAD2	297	1	326	337	338	327			
148-	CQUAD2	298	1	327	338	339	328			
149-	CQUAD2	299	1	328	339	340	329			
150-	CQUAD2	300	1	329	340	341	330			

PLATE TRANSIENT RESPONSE

SORTED BULK DATA ECHO

CARD COUNT	. 1 ..	2 ..	3 ..	4 ..	5 ..	6 ..	7 ..	8 ..	9 ..	10 .
151-	CQUAD2	306	1	336	347	348	337			
152-	CQUAD2	307	1	337	348	349	338			
153-	CQUAD2	308	1	338	349	350	339			
154-	CQUAD2	309	1	339	350	351	340			
155-	CQUAD2	310	1	340	351	352	341			
156-	CQUAD2	316	1	347	358	359	348			
157-	CQUAD2	317	1	348	359	360	349			
158-	CQUAD2	318	1	349	360	361	350			
159-	CQUAD2	319	1	350	361	362	351			
160-	CQUAD2	320	1	351	362	363	352			
161-	CQUAD2	326	1	358	369	370	359			
162-	CQUAD2	327	1	359	370	371	360			
163-	CQUAD2	328	1	360	371	372	361			
164-	CQUAD2	329	1	361	372	373	362			
165-	CQUAD2	330	1	362	373	374	363			
166-	DAREA	65	171	3	230.					
167-	EIGR	1	INV	.0	15000.	11	11			+EI
168-	+EI	MAX								
169-	GRDSET							6		
170-	GRID	6		.0000	.0000	.0000				
171-	GRID	7		.0000	.3000	.0000				
172-	GRID	8		.0000	.6000	.0000				
173-	GRID	9		.0000	.9000	.0000				
174-	GRID	10		.0000	1.2000	.0000				
175-	GRID	11		.0000	1.5000	.0000				
176-	GRID	17		.3000	.0000	.0000				
177-	GRID	18		.3000	.3000	.0000				
178-	GRID	19		.3000	.6000	.0000				
179-	GRID	20		.3000	.9000	.0000				
180-	GRID	21		.3000	1.2000	.0000				
181-	GRID	22		.3000	1.5000	.0000				
182-	GRID	28		.6000	.0000	.0000				
183-	GRID	29		.6000	.3000	.0000				
184-	GRID	30		.6000	.6000	.0000				
185-	GRID	31		.6000	.9000	.0000				
186-	GRID	32		.6000	1.2000	.0000				
187-	GRID	33		.6000	1.5000	.0000				
188-	GRID	39		.9000	.0000	.0000				
189-	GRID	40		.9000	.3000	.0000				
190-	GRID	41		.9000	.6000	.0000				
191-	GRID	42		.9000	.9000	.0000				
192-	GRID	43		.9000	1.2000	.0000				
193-	GRID	44		.9000	1.5000	.0000				
194-	GRID	50		1.2000	.0000	.0000				
195-	GRID	51		1.2000	.3000	.0000				
196-	GRID	52		1.2000	.6000	.0000				
197-	GRID	53		1.2000	.9000	.0000				
198-	GRID	54		1.2000	1.2000	.0000				
199-	GRID	55		1.2000	1.5000	.0000				
200-	GRID	61		1.5000	.0000	.0000				

PLATE TRANSIENT RESPONSE

SORTED BULK DATA ECHO

CARD COUNT	. 1 ..	2 ..	3 ..	4 ..	5 ..	6 ..	7 ..	8 ..	9 ..	10 .
201-	GRID	62		1.5000	.3000	.0000				
202-	GRID	63		1.5000	.6000	.0000				
203-	GRID	64		1.5000	.9000	.0000				
204-	GRID	65		1.5000	1.2000	.0000				
205-	GRID	66		1.5000	1.5000	.0000				
206-	GRID	72		1.6500	.0000	.0000				
207-	GRID	73		1.6500	.3000	.0000				
208-	GRID	74		1.6500	.6000	.0000				
209-	GRID	75		1.6500	.9000	.0000				
210-	GRID	76		1.6500	1.2000	.0000				
211-	GRID	77		1.6500	1.5000	.0000				
212-	GRID	83		1.8000	.0000	.0000				
213-	GRID	84		1.8000	.3000	.0000				
214-	GRID	85		1.8000	.6000	.0000				
215-	GRID	86		1.8000	.9000	.0000				
216-	GRID	87		1.8000	1.2000	.0000				
217-	GRID	88		1.8000	1.5000	.0000				
218-	GRID	94		1.9500	.0000	.0000				
219-	GRID	95		1.9500	.3000	.0000				
220-	GRID	96		1.9500	.6000	.0000				
221-	GRID	97		1.9500	.9000	.0000				
222-	GRID	98		1.9500	1.2000	.0000				
223-	GRID	99		1.9500	1.5000	.0000				
224-	GRID	105		2.1000	.0000	.0000				
225-	GRID	106		2.1000	.3000	.0000				
226-	GRID	107		2.1000	.6000	.0000				
227-	GRID	108		2.1000	.9000	.0000				
228-	GRID	109		2.1000	1.2000	.0000				
229-	GRID	110		2.1000	1.5000	.0000				
230-	GRID	116		2.2500	.0000	.0000				
231-	GRID	117		2.2500	.3000	.0000				
232-	GRID	118		2.2500	.6000	.0000				
233-	GRID	119		2.2500	.9000	.0000				
234-	GRID	120		2.2500	1.2000	.0000				
235-	GRID	121		2.2500	1.5000	.0000				
236-	GRID	127		2.4000	.0000	.0000				
237-	GRID	128		2.4000	.3000	.0000				
238-	GRID	129		2.4000	.6000	.0000				
239-	GRID	130		2.4000	.9000	.0000				
240-	GRID	131		2.4000	1.2000	.0000				
241-	GRID	132		2.4000	1.5000	.0000				
242-	GRID	138		2.5500	.0000	.0000				
243-	GRID	139		2.5500	.3000	.0000				
244-	GRID	140		2.5500	.6000	.0000				
245-	GRID	141		2.5500	.9000	.0000				
246-	GRID	142		2.5500	1.2000	.0000				
247-	GRID	143		2.5500	1.5000	.0000				
248-	GRID	149		2.7000	.0000	.0000				
249-	GRID	150		2.7000	.3000	.0000				
250-	GRID	151		2.7000	.6000	.0000				

PLATE TRANSIENT RESPONSE

SORTED BULK DATA ECHO

CARD COUNT	. 1 ..	2 ..	3 ..	4 ..	5 ..	6 ..	7 ..	8 ..	9 ..	10 .
251-	GRID	152		2.7000	.9000	.0000				
252-	GRID	153		2.7000	1.2000	.0000				
253-	GRID	154		2.7000	1.5000	.0000				
254-	GRID	160		2.8500	.0000	.0000				
255-	GRID	161		2.8500	.3000	.0000				
256	GRID	162		2.8500	.6000	.0000				
257-	GRID	163		2.8500	.9000	.0000				
258-	GRID	164		2.8500	1.2000	.0000				
259-	GRID	165		2.8500	1.5000	.0000				
260-	GRID	171		3.0000	.0000	.0000				
261-	GRID	172		3.0000	.3000	.0000				
262-	GRID	173		3.0000	.6000	.0000				
263-	GRID	174		3.0000	.9000	.0000				
264-	GRID	175		3.0000	1.2000	.0000				
265-	GRID	176		3.0000	1.5000	.0000				
266-	GRID	182		3.1500	.0000	.0000				
267-	GRID	183		3.1500	.3000	.0000				
268-	GRID	184		3.1500	.6000	.0000				
269-	GRID	185		3.1500	.9000	.0000				
270-	GRID	186		3.1500	1.2000	.0000				
271-	GRID	187		3.1500	1.5000	.0000				
272-	GRID	193		3.3000	.0000	.0000				
273-	GRID	194		3.3000	.3000	.0000				
274-	GRID	195		3.3000	.6000	.0000				
275-	GRID	196		3.3000	.9000	.0000				
276-	GRID	197		3.3000	1.2000	.0000				
277-	GRID	198		3.3000	1.5000	.0000				
278-	GRID	204		3.4500	.0000	.0000				
279-	GRID	205		3.4500	.3000	.0000				
280-	GRID	206		3.4500	.6000	.0000				
281-	GRID	207		3.4500	.9000	.0000				
282-	GRID	208		3.4500	1.2000	.0000				
283-	GRID	209		3.4500	1.5000	.0000				
284-	GRID	215		3.6000	.0000	.0000				
285-	GRID	216		3.6000	.3000	.0000				
286-	GRID	217		3.6000	.6000	.0000				
287-	GRID	218		3.6000	.9000	.0000				
288-	GRID	219		3.6000	1.2000	.0000				
289-	GRID	220		3.6000	1.5000	.0000				
290-	GRID	226		3.7500	.0000	.0000				
291-	GRID	227		3.7500	.3000	.0000				
292-	GRID	228		3.7500	.6000	.0000				
293-	GRID	229		3.7500	.9000	.0000				
294-	GRID	230		3.7500	1.2000	.0000				
295-	GRID	231		3.7500	1.5000	.0000				
296-	GRID	237		3.9000	.0000	.0000				
297-	GRID	238		3.9000	.3000	.0000				
298-	GRID	239		3.9000	.6000	.0000				
299-	GRID	240		3.9000	.9000	.0000				
300-	GRID	241		3.9000	1.2000	.0000				

PLATE TRANSIENT RESPONSE

SORTED BULK DATA ECHO

CARD COUNT	. 1 ..	2 ..	3 ..	4 ..	5 ..	6 ..	7 ..	8 ..	9 ..	10 .
301-	GRID	242		3.9000	1.5000	.0000				
302-	GRID	248		4.0500	.0000	.0000				
303-	GRID	249		4.0500	.3000	.0000				
304-	GRID	250		4.0500	.6000	.0000				
305-	GRID	251		4.0500	.9000	.0000				
306-	GRID	252		4.0500	1.2000	.0000				
307-	GRID	253		4.0500	1.5000	.0000				
308-	GRID	259		4.2000	.0000	.0000				
309-	GRID	260		4.2000	.3000	.0000				
310-	GRID	261		4.2000	.6000	.0000				
311-	GRID	262		4.2000	.9000	.0000				
312-	GRID	263		4.2000	1.2000	.0000				
313-	GRID	264		4.2000	1.5000	.0000				
314-	GRID	270		4.3500	.0000	.0000				
315-	GRID	271		4.3500	.3000	.0000				
316-	GRID	272		4.3500	.6000	.0000				
317-	GRID	273		4.3500	.9000	.0000				
318-	GRID	274		4.3500	1.2000	.0000				
319-	GRID	275		4.3500	1.5000	.0000				
320-	GRID	281		4.5000	.0000	.0000				
321-	GRID	282		4.5000	.3000	.0000				
322-	GRID	283		4.5000	.6000	.0000				
323-	GRID	284		4.5000	.9000	.0000				
324-	GRID	285		4.5000	1.2000	.0000				
325-	GRID	286		4.5000	1.5000	.0000				
326-	GRID	292		4.8125	.0000	.0000				
327-	GRID	293		4.8125	.3000	.0000				
328-	GRID	294		4.8125	.6000	.0000				
329-	GRID	295		4.8125	.9000	.0000				
330-	GRID	296		4.8125	1.2000	.0000				
331-	GRID	297		4.8125	1.5000	.0000				
332-	GRID	303		5.1250	.0000	.0000				
333-	GRID	304		5.1250	.3000	.0000				
334-	GRID	305		5.1250	.6000	.0000				
335-	GRID	306		5.1250	.9000	.0000				
336-	GRID	307		5.1250	1.2000	.0000				
337-	GRID	308		5.1250	1.5000	.0000				
338-	GRID	314		5.4375	.0000	.0000				
339-	GRID	315		5.4375	.3000	.0000				
340-	GRID	316		5.4375	.6000	.0000				
341-	GRID	317		5.4375	.9000	.0000				
342-	GRID	318		5.4375	1.2000	.0000				
343-	GRID	319		5.4375	1.5000	.0000				
344-	GRID	325		5.7500	.0000	.0000				
345-	GRID	326		5.7500	.3000	.0000				
346-	GRID	327		5.7500	.6000	.0000				
347-	GRID	328		5.7500	.9000	.0000				
348-	GRID	329		5.7500	1.2000	.0000				
349-	GRID	330		5.7500	1.5000	.0000				
350-	GRID	336		6.0625	.0000	.0000				

PLATE TRANSIENT RESPONSE

SORTED BULK DATA ECHO

CARD COUNT	. 1 ..	2 ..	3 ..	4 ..	5 ..	6 ..	7 ..	8 ..	9 ..	10 .
351-	GRID	337		6.0625	.3000	.0000				
352-	GRID	338		6.0625	.6000	.0000				
353-	GRID	339		6.0625	.9000	.0000				
354-	GRID	340		6.0625	1.2000	.0000				
355-	GRID	341		6.0625	1.5000	.0000				
356-	GRID	347		6.3750	.0000	.0000				
357-	GRID	348		6.3750	.3000	.0000				
358-	GRID	349		6.3750	.6000	.0000				
359-	GRID	350		6.3750	.9000	.0000				
360-	GRID	351		6.3750	1.2000	.0000				
361-	GRID	352		6.3750	1.5000	.0000				
362-	GRID	358		6.6875	.0000	.0000				
363-	GRID	359		6.6875	.3000	.0000				
364-	GRID	360		6.6875	.6000	.0000				
365-	GRID	361		6.6875	.9000	.0000				
366-	GRID	362		6.6875	1.2000	.0000				
367-	GRID	363		6.6875	1.5000	.0000				
368-	GRID	369		7.0000	.0000	.0000				
369-	GRID	370		7.0000	.3000	.0000				
370-	GRID	371		7.0000	.6000	.0000				
371-	GRID	372		7.0000	.9000	.0000				
372-	GRID	373		7.0000	1.2000	.0000				
373-	GRID	374		7.0000	1.5000	.0000				
374-	MAT1	1	1.+7		.3	.2587E-3				
375-	PARAM	LMODES	10							
376-	PQUAD2	1	1	.1875						
377-	SPC1	2	4	17	28	39	50	61	72	+A2
378-	+A2	83	94	105	116	127	138	149	160	+B2
379-	+B2	171	182	193	204	215	226	237	248	+C2
380-	+C2	259	270	281	292	303	314	325	336	+D2
381-	+D2	347	358	369						
382-	SPC1	2	123456	6	THRU	11				
383-	TABLED1	75								+A75
384-	+A75	0.0	0.0	3.0-6	0.1705	6.0-6	0.3360	9.0-6	0.4917	+B75
385-	+B75	12.0-6	0.6330	15.0-6	0.7557	18.0-6	0.8563	21.0-6	0.9319	+C75
386-	+C75	24.0-6	0.9801	27.0-6	0.9996	27.5-6	1.0000	28.0-6	0.9996	+D75
387-	+D75	31.0-6	0.9801	34.0-6	0.9319	37.0-6	0.8563	40.0-6	0.7557	+E75
388-	+E75	43.0-6	0.6330	46.0-6	0.4917	49.0-6	0.3360	52.0-6	0.1705	+F75
389-	+F75	55.0-6	0.0000	ENDT						
390-	TLOAD1	70	65			75				
391-	TSTEP	60	55	1.0-6	1					
	ENDDATA									

☆ U. S. GOVERNMENT PRINTING OFFICE: 1976 — 657-630/1013